UCRL 3374

UNIVERSITY OF CALIFORNIA

Radiation Laboratory

I. EXPERIMENTAL STUDY OF NUCLEAR ISOMERS IN THE MILLIMICROSECOND LIFETIME RANGE

II. APPLICATIONS OF NILSSON'S WAVE FUNCTIONS FOR DEFORMED NUCLEI

TWO-WEEK LOAN COPY

This is a Library Circulating Copy which may be borrowed for two weeks. For a personal retention copy, call Tech. Info. Division, Ext. 5545

DISCLAIMER

This document was prepared as an account of work sponsored by the United States Government. While this document is believed to contain correct information, neither the United States Government nor any agency thereof, nor the Regents of the University of California, nor any of their employees, makes any warranty, express or implied, or assumes any legal responsibility for the accuracy, completeness, or usefulness of any information, apparatus, product, or process disclosed, or represents that its use would not infringe privately owned rights. Reference herein to any specific commercial product, process, or service by its trade name, trademark, manufacturer, or otherwise, does not necessarily constitute or imply its endorsement, recommendation, or favoring by the United States Government or any agency thereof, or the Regents of the University of California. The views and opinions of authors expressed herein do not necessarily state or reflect those of the United States Government or any agency thereof or the Regents of the University of California.

UCRL-3374

UNIVERSITY OF CALIFORNIA
Radiation Laboratory
Berkeley, California

Contract No. W-7405-eng-48

I. EXPERIMENTAL STUDY OF NUCLEAR ISOMERS IN THE MILLIMICROSECOND LIFETIME RANGE

II. APPLICATIONS OF NILSSON'S WAVE FUNCTIONS FOR DEFORMED NUCLEI

Donald Strominger

(Thesis)

June, 1956

Printed for the U. S. Atomic Energy Commission

I. EXPERIMENTAL STUDY OF NUCLEAR ISOMERS IN THE MILLIMICROSECOND LIFETIME RANGE

II. APPLICATIONS OF NILSSON'S WAVE FUNCTIONS FOR DEFORMED NUCLEI

Contents

Abstract 4

I. Experimental Study of Nuclear Isomers in the Millimicrosecond Lifetime Range

A. Introduction 5

B. Experimental Techniques

1. Radiation Detectors 7
2. The Fast-Slow Coincidence Circuit 9
3. The Method of Delayed Coincidences 12
4. General Considerations of Delay Curves 13

C. Experimental Results

1. Electric Dipole Transitions
   - a. Am^{243} Decay 15
   - b. Ra^{225} Decay 15
   - c. Np^{237} Decay 17
   - d. Th^{231} Decay 20
   - e. Cf^{249} Decay 25
   - f. Th^{227} Decay 25
   - g. U^{235} Decay 27
   - h. Tl^{209} Decay 27
   - i. U^{230} Family Decay 34
2. Magnetic Dipole Transitions
   - a. Cm^{243} Decay 36
   - b. Bi^{213} Decay 38
   - c. Re^{183} Decay 38
   - d. Pa^{231} Decay 38
3. Electric Quadrupole Transitions
   - a. U^{230} Family Decay 40
   - b. Re^{184} Decay 40
   - c. Fr^{221} Decay 44

4. Other Results 45

D. Discussion of Results

1. Electric Dipole Transitions

a. Tl^{209} Decay 47

b. 1- States 49

2. Magnetic Dipole Transitions 49

3. Electric Quadrupole Transitions 52

4. Levels of W^{184} Populated by Decay of Re^{184} . . 53

II. Applications of Nilsson's Wave Functions for Deformed Nuclei

A. Introduction 56

B. Applications

1. Decoupling Parameters 60

2. Magnetic Moments. 63

3. Electric Dipole Transition Probabilities . . . 71

C. Discussion of Results

1. Assignments of Ground State Spins 79

2. Decoupling Parameters and Magnetic Moments 79

3. Electric Dipole Transition Probabilities . . . 81

D. Acknowledgments 87

References 88

I. EXPERIMENTAL STUDY OF NUCLEAR ISOMERS IN THE MILLIMICROSECOND LIFETIME RANGE

II. APPLICATIONS OF NILSSON'S WAVE FUNCTIONS FOR DEFORMED NUCLEI

Donald Strominger

Radiation Laboratory and
Department of Chemistry and Chemical Engineering
University of California, Berkeley, California

April 13, 1956

ABSTRACT

The method of delayed coincidences was used to search for metastable states with half-lives in the millimicrosecond range Metastable states were found in the following daughter nuclei: Pa^{231} $t_{1/2} = 4.1 \pm .4 \times 10^{-8}$ sec, Pb^{209}, $t_{1/2} = 3.1 \pm 1.0 \times 10^{-9}$ sec, and W^{184}, $t_{1/2} = 9 \pm 3 \times 10^{-10}$ sec. In addition, the existence of short-lived metastable states in the daughter nuclides Pa^{233} and Pu^{239} was confirmed. Upper limits for the half-lives of other gamma transitions were set. A decay scheme for Re^{184} is proposed.

Several critical tests of Nilsson's wave functions were made for strongly deformed nuclei. The wave functions were used to calculate decoupling parameters, magnetic moments, and E1 transition probabilities. These calculated nuclear properties are compared with experimental data in the heavy element region. The calculated values are found to be generally in qualitative agreement with the experimental data. Nilsson's orbits are correlated with nuclear ground-state spins in the actinide region. New selection rules for E1 transitions are discussed.

I. EXPERIMENTAL STUDY OF NUCLEAR ISOMERS IN THE MILLIMICROSECOND LIFETIME REGION

A. Introduction

A nuclear metastable state may be defined as an excited state of a nucleus which exists for a measurable length of time. With present delayed-coincidence techniques it is possible to measure half-lives as short as a few hundredths of a millimicrosecond.[1]

Excited nuclear states may decay by the emission of gamma radiation or by the ejection of an orbital electron. It is convenient to classify electromagnetic radiation by multipole order L, according to the angular momenta L (in units of $\hbar$) carried by the radiation. There are two classes of multipole order, EL (electric) and ML (magnetic), which differ with respect to parity. The conservation of angular momentum and parity imposes certain selection rules on the possible multipolarities of a gamma transition between two states of specified angular momenta (I_i, I_f) and parities (π_i, π_f):[2]

$$|I_i - I_f| \leq L \leq I_i + I_f , \tag{1}$$

$$\Delta\pi = \frac{\pi_i}{\pi_f} = (-1)^L \text{ for EL radiation}$$
$$= (-1)^{L+1} \text{ for ML radiation.}$$

Here $\Delta\pi = -1$ denotes a parity change.

The transition probability for the decay of an excited nuclear state by gamma radiation depends upon the multipolarity and energy of the radiations and also on the wave functions of the nuclear states involved in the transition.[2] Formulae for estimating the transition probabilities of various multipole radiations have been given by Weisskopf.[2, 3] These formulae were obtained on the assumption that the radiations were due to single-particle transitions. Unfortunately the formulae are of little value in determining multipolarities. A particular transition may be highly hindered if there is little overlap between the wave functions of the nuclear states involved.[4] On the

other hand, certain transition probabilities are greatly enhanced by a "cooperative" phenomenon of many nucleons.[4-6] It is still convenient to compare experimental half lives with the values calculated from the Weisskopf formulae.[2-4]

Internal conversion coefficients depend on the energy and multipolarity of the radiation, and the particular atomic orbitals and wave functions of the electrons involved, but not on the wave functions of the nuclear levels.[2] Therefore, relative and absolute internal conversion coefficients can be used to determine multipole orders of radiation.

Consider a nuclear level and let

T_{level} = mean life of the level,

T_r = partial mean life of the gamma radiations from the level,

T_{e^-} = partial mean life of the conversion electrons from the level,

N_r = relative number of gamma rays emitted,

N_{e^-} = relative number of total conversion electrons emitted,

α = total conversion coefficient.

Then $$\frac{1}{T_{level}} = \frac{1}{T_r} + \frac{1}{T_{e^-}} . \qquad (2)$$

By definition $\alpha = \frac{N_{e^-}}{N_r} = \frac{T_r}{T_{e^-}}$.

Therefore $$\frac{1}{T_{level}} = \frac{1}{T_r} \left(1 + \frac{N_{e^-}}{N_r}\right) = \frac{1}{T_r} (1 + \alpha). \qquad (2)$$

From this result we see that the transition probability of the level is enhanced by a factor of $(1 + \alpha)$ because of the internal conversion process. This formula also relates the experimentally determined half life with the partial half life of the gamma radiation.

Nuclear isomeric states play a significant role in the understanding of the details of nuclear structure. From the multipole character and the transition probabilities of gamma radiations, many checks on the validity of existing nuclear models can be made.[4-6]

The metastable state must be reached as a product of a radioactive disintegration. As an illustration, let us consider alpha decay to an excited state. The alpha particles, and gamma rays from the excited state, will not be emitted simultaneously, but there will be a time interval between the alpha-particle and the gamma-ray emission. Experimentally, the problem is to measure this time interval. In this study the method of delayed coincidences was employed for this purpose.

Only metastable states with half lives in the millimicrosecond region were sought. This immediately restricts us to transitions with multipolarities E1, M1, E2, or M2. Any higher-order multipole transition would have a half life so much longer that it would not be in the millimicrosecond region unless the energy of the transition were very large.[2, 3]

There are other ways of deducing transition probabilities of gamma transitions besides direct lifetime measurement (coulombic excitation,[6, 7] competition of gamma radiation with other processes like alpha emission,[8] etc.). The coulombic excitation process has proved useful for measuring electric quadrupole transition probabilities which directly populate the ground state.[5-7] The methods of delayed coincidences and coulombic excitation compliment each other in that the latter method is easier to apply when the transition probability is large, while the former is more useful for transitions with small transition probabilities.

B. Experimental Techniques

1. Radiation Detectors

Scintillation detectors were used to detect all types of radiation emitted from nuclei. They offer the advantages of short resolving times while there is still a reasonable measure of the energy of the detected radiation.[9] The type of phosphor used in the scintillation detector varied with the nature of the radiation and the specific experiment being carried out.

To detect alpha particles both potassium iodide[9] (thallium iodide activated) and stilbene[9] scintillation crystals were used. Potassium iodide crystals were used only when it was desired to resolve alpha radiation from a high beta or gamma background. These crystals were about 1 cm square and about 2 mm thick. For our purposes the crystals were usually cleaved on five sides. The crystals were then fastened directly to the window of an RCA-5819 photomultiplier tube with a vaseline seal. The resolution obtained with potassium iodide crystals prepared in this manner was more than sufficient to resolve alpha particles from other high-energy radiation present.

When it was not necessary to resolve alpha radiation from other radiation, a stilbene crystal was used, which was prepared in the following manner. A lucite disc approximately 5 cm in diameter and 2 cm thick was shaped on one end to fit the window of an RCA 5819 photomultiplier tube. A well was drilled on the other face of the disc about 1 cm in depth and 3 cm in diameter. Enough trans-stilbene was sublimed to form a thin layer of the material on the inside of the well. The disc was then fastened with a vaseline seal to an RCA 5819 photomultiplier tube.

Sodium iodide (thallium iodide activated) crystals[9] were used for the detection and analysis of electromagnetic radiation. By nature sodium iodide is hygroscopic; therefore, it is necessary to protect the crystal from the atmosphere. This was done by placing the crystal in an aluminum can with a thin beryllium window on one face and a thin quartz window on the other. The quartz was preshaped to fit an RCA 5819 photomultiplier tube. Magnesium oxide was placed between the metal shield and the sodium iodide crystal to act as a light reflector. The optical contact was made with Dow Corning 200 Fluid. The sodium iodide crystals used were 1.5 in. in diameter by 1 in. in thickness. Kalkstein and Hollander[10] have thoroughly reviewed the literature on the subject of the counting efficiency of a sodium iodide crystal with the above dimensions. The curves given in that reference were used to correct for the photopeak counting efficiency.

2. The Fast-Slow Coincidence Circuit

A block diagram of the coincidence circuit is shown in Fig. 1. In order to get the shortest possible rise time for the electronic pulses, it is desirable to maintain a very high voltage on the RCA 5819 photomultiplier tubes. Thus 1100 volts were usually applied to the 5819 photomultiplier tubes.

The pulses, at this point negative, are sent from the photomultiplier tubes through a preamplifier and cathode follower. Here the pulses are branched. For the fast-coincidence part they are passed through two or three Hewlett-Packard 460A Wide Band Amplifiers (modified). To ensure maximum gain in these amplifiers only 5654 tubes with a transconductance greater than four thousand micromhos were used. To prevent positive pulses from entering the fast-coincidence circuit General Electric G7A diodes were placed on the outputs of the wide-band amplifiers. From the wide-band amplifiers the pulses are led into a delay box. This delay box consists of measured lengths of RG-63/U or Amphenol 21 342 cable. Both of these cables have a nominal propagation factor of about 0.84. That is, one foot of this cable will delay a pulse 1.21 millimicroseconds. This value was checked experimentally by searching for resonant frequencies in open and shorted cables of the delay box. The results obtained were in reasonable agreement with the above value. From the delay box the pulses are fed into the "fast" coincidence circuit.

A schematic diagram of the "fast" coincidence circuit is shown in Fig. 2. The pulses are flattened and converted into positive pulses by balanced 404A pentodes. Next the pulses are shaped to 0.01 to 0.04 microsecond by a shorted 200-ohm cable. Thus the resolving time of the fast-coincidence circuit is 0.02 to 0.08 μsec (the sum of the widths of the shaped pulses in each channel). A bias is placed on the first G7A diode sufficient that if a pulse comes from only one of the channels it will not overcome the bias, but if two pulses are in coincidence the composite pulse is larger than the bias on the diode. The rest of this circuit is designed to generate a uniform pulse whenever there is a fast coincidence at the G7A diode. This output pulse is fed

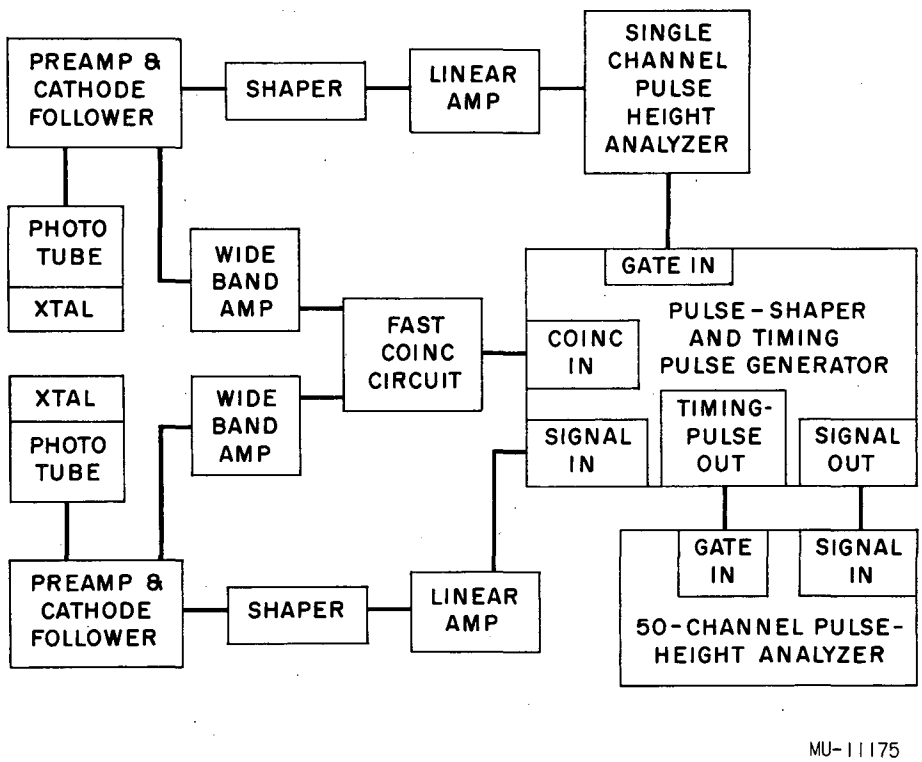

Fig. I-1 Block Diagram of Fast-Slow Coincidence Circuit

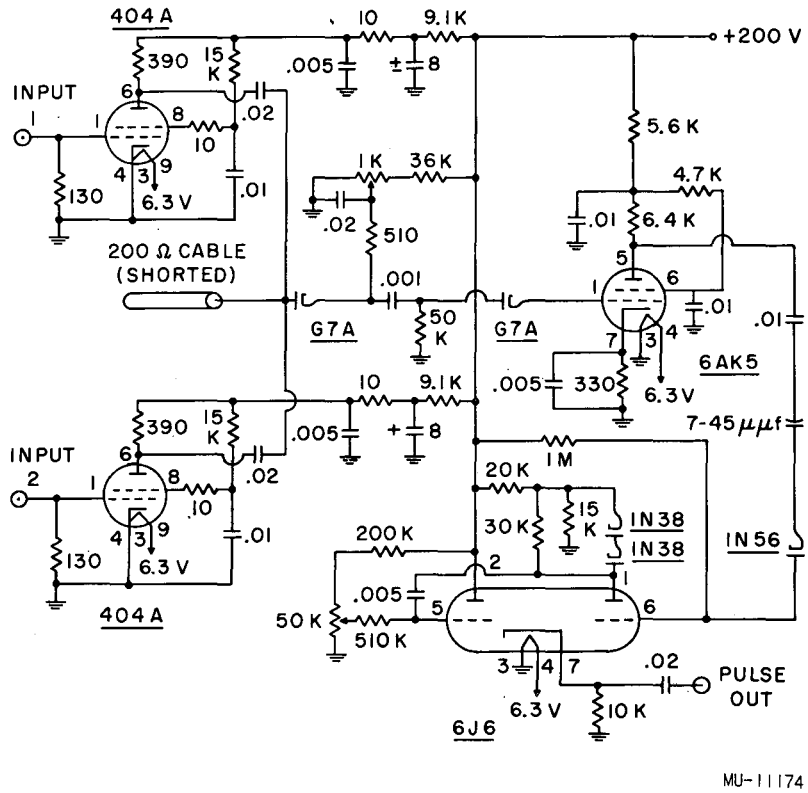

Fig. I-2 Schematic Diagram of Fast Coincidence Circuit

into the "coinc in" part of the triple-coincidence circuit of the "pulse shaper and timing-pulse generator."

The other branch of the pulse from the cathode follower on the gate side goes through a shaper where it is shaped to about 2 μsec. It is amplified and converted into a positive pulse in a linear amplifier and then analyzed by a Los Alamos-type single-channel pulse-height analyzer.[11] The selected pulses from this analyzer are fed into the "gate in" part of the slow triple-coincidence circuit of the pulse shaper and timing-pulse generator.

The other part of the pulse from the cathode follower on the signal side is shaped to about 2 μsec, amplified, and converted into a positive pulse in a linear amplifier and then fed into the pulse shaper and timing-pulse generator. Here part of the signal pulse is used to trigger a multivibrator which sends its pulse to the triple-coincidence circuit. The rest of the signal pulse is shaped to about 10 μsec and fed into the signal input of the 50-channel pulse-height analyzer.[12] If the pulses from the single-channel pulse-height analyzer, fast-coincidence circuit, and the multivibrator in the pulse shaper arrive at the triple-coincidence circuit within its resolving time (about 2 μsec), a timing pulse is generated which is used to gate the 50-channel pulse-height analyzer.

3. The Method of Delayed Coincidences

The method of delayed coincidences as it applies to measurement of the lifetime of a particular nuclear state is performed as follows. The proper scintillation detector is chosen for the initial radiation (which may be alpha particles, beta particles, K x-rays following electron capture, or a gamma transition which precedes the transition of interest). The electronic pulses resulting from this initial radiation are selected by the single-channel pulse-height analyzer. The succeeding radiation is detected on the signal counter and the gains of the various amplifiers adjusted so that its energy spectrum appears on the 50-channel pulse-height analyzer. The rest of the experiment consists of determining the coincidence-counting rate as a function of electronic delay.

A plot of the coincidence-counting rate as a function of delay is conveniently made on semilogarithmic graph paper. We shall henceforth call such a graph a delay curve. To determine the lower limit of half-life detection it is necessary to run a "prompt" delay curve. That is, a delay curve must be run where it is known that the succeeding radiation is prompt ($t_{1/2} < 10^{-11}$ sec) with regard to the initial radiation. The two 510-kev annihilation radiations accompanying the positron decay of Na^{22} were used to show that the optimum lower limit of half-life measurement with this equipment is about 0.8 mμsec. This latter figure is the actual finite slope shown by prompt delay curves. Unfortunately the finite slope seems to be energy-dependent, and the optimum lower limit for low-energy radiations is somewhat more than 0.8 mμsec. The upper limit of half-life detection is determined by the resolving time of the fast-coincidence circuit. Thus, with our resolving time of 0.02 to 0.08 μsec, the upper limit is about 1 μsec.

Random coincidence rates were usually obtained by inserting a long delay (about 160 mμsec) between the Hewlett-Packard amplifiers and the fast-coincidence circuit on the signal channel. The chance counting rate thus obtained was usually negligible compared to the prompt true coincidence counting rate.

4. General Considerations of Delay Curves

The nature of the delay curve obtained in a particular experiment is a function of several variables. The one over which we have the least control is the energy of the radiations in coincidence with the gating event.

From the description of the electronics equipment we see that the final pulses used for the fast-coincidence circuit are shaped by a process of reflection. Thus the time displacement of these pulses relative to the gating event will be a function of the rise times of the initial pulses, which are functions of the energy of the radiations. Low-energy radiations have longer rise times; therefore, the entire delay curves of these lower-energy radiations will be displaced from the delay curves of higher-energy radiations.

As a consequence of the above it is essential to have each counter count radiation of only a single energy at any one time. It is also important when comparing an experimental delay curve with a "prompt" delay curve to have the energies of the two gating radiations and the two coincident radiations as close as possible for the purposes of this comparison.

For half lives that are long compared to the finite slope of a prompt delay curve, the trailing edge of the delay curve becomes an exponential whose slope is determined by the half life or half lives of the coincident radiation.[13-16] If the half life of the radioactive transition is about the same as the finite slope of a prompt delay curve, then a more detailed analysis of the delay curve is necessary. Much work has been done on the statistical theory of delayed-coincidence experiments.[14-16] This work has deduced theoretical equations which correlate "prompt" coincidence curves with "delayed" coincidence curves when the coincident radiation has a measurable half life.[14,15]

If the half life of a coincident radiation is too short to be measured by the exponential slope of the delay curve, but is long enough to cause a displacement of the delay curve, the half life may be calculated by methods suggested by Newton[15] and Bay.[14] A method similar to Newton's[15] was used to evaluate the half life of the 1.1 mμsec metastable state following Cm^{243} alpha decay, and Bay's method[14] was used to calculate the half life of the 111.2-kev level following the electron-capture decay of Re^{184}.

Other interesting properties of delay curves are enumerated and discussed in more detail by Newton,[15] and also by Bell et al.[13]

C. Experimental Results

1. Electric Dipole Transitions

The lifetime measurements of E1 transitions in the heavy region has been of considerable interest ever since Beling, Newton, and Rose[17] discovered the measurable half life of the 59.7-kev E1 transition following the alpha decay of Am^{241} to Np^{237}. Stephens[18]

has tabulated many of the E1 transitions known in the odd-mass nuclei in the translead region and the measurement of the lifetimes of most of these transitions has now been completed either in this study or by the work of others.[18-21]

Stephens[18] has also reported the existence of several low-lying odd-parity states in even-even nuclei which decay by E1 transitions. Several of these particular transitions were also studied. The results of the measurements on odd-mass nuclides in the deformed region are discussed in the section dealing with Nilsson's wave functions. The rest of the data are covered in the section on discussion of results for Part I.

a. Am^{243} decay. The isotope Am^{243} is prepared by the intense neutron irradiation of lower elements, ultimately uranium.[22, 23] The samples used for the following study had one hundred times as much Am^{243} as Am^{241} by activity. This activity was placed on thin aluminum plates.

Of interest here is a 75-kev transition following the alpha decay of Am^{243} assigned as E1 on the basis of conversion coefficients.[24] Since the analogous 59.7-kev E1 transition following the alpha decay of Am^{241} has a half life of 63 mμsec,[17] we would expect the E1 transition in Np^{239} to have some similar half life.

Figure 3 shows a delay curve of the 75-kev radiation coincident with alpha particles. A potassium iodide crystal was used for the detection of alpha particles and a sodium iodide crystal was used for gamma-ray detection and analysis. As a result of this run we may set an upper limit of 1.6 mμsec for the half life of the 75-kev transition. This result is in agreement with the results of Kalkstein and Rasmussen[25] and also those of Engelkemeir,[26] who were able to set an upper limit of 2 mμsec for the half life. They studied this E1 transition following the beta decay of U^{239} to Np^{239}.

b. Ra^{225} decay. Ra^{225} is a beta emitter with a 14.8-day half life.[22] It may be prepared from the natural radioactive product Th^{229}. Chemical purification of this isotope is simple. It consists of an extraction of aqueous Th^{229} solution with 0.4 M TTA (thenoyltrifluoroacetone) solution in benzene. The acidity of the

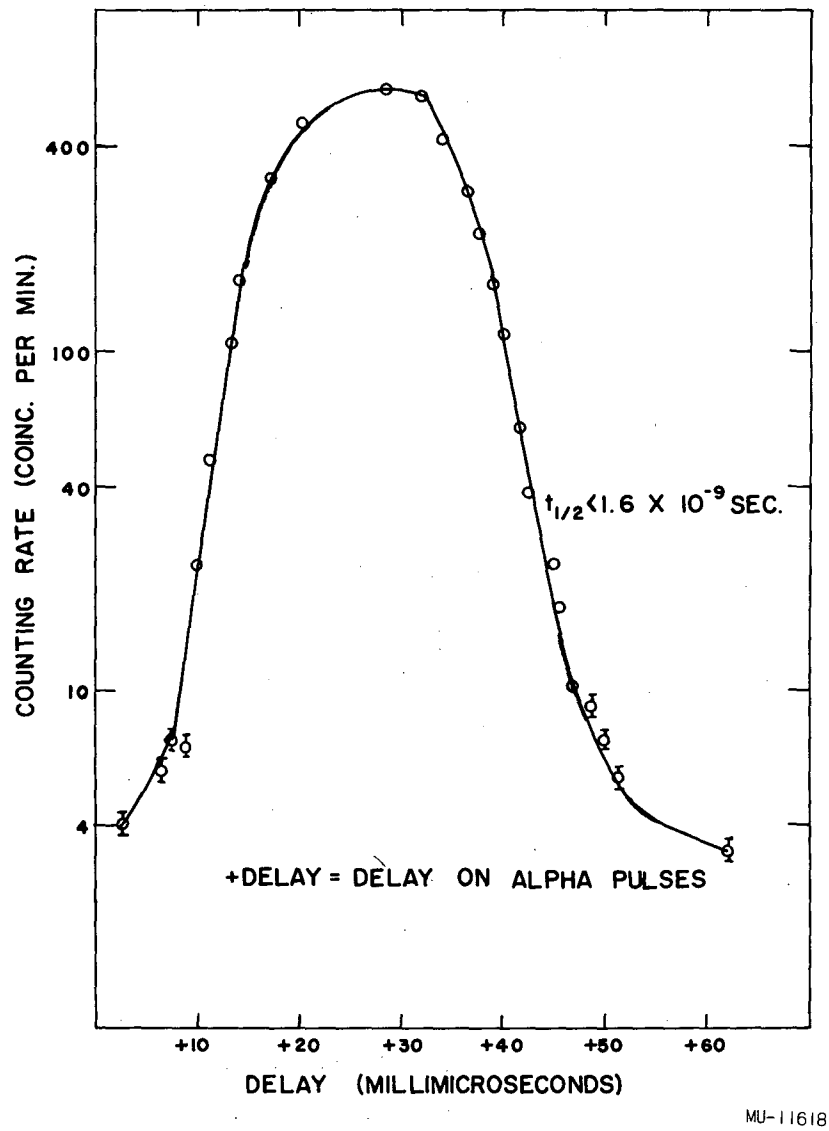

Fig. I-3 Delay Curve of 75-kev E1 Transition Following Am^{243} Alpha Decay

aqueous phase is adjusted to a pH of about 5. Under these conditions the Ra^{225} activity remains in the aqueous phase while all the other activities present in the Th^{229} decay chain extract into the benzene phase. Ra^{225} activity prepared in the above manner was mounted on a thin aluminum disc.

The main point of interest here was to study the lifetime of the 40-kev transition following the beta decay of Ra^{225}. Stephens[18] has assigned this transition as E1 on the basis of total and L-subshell conversion coefficients. The level giving rise to the 27-kev E1 transition following alpha decay of Pa^{231} to Ac^{227} has been found to be metastable, with a half life of about 40 mμsec.[20] Since Ra^{225} beta-decays to the analogous daughter, Ac^{225}, it is reasonable to expect the 40-kev E1 transition to be delayed in a manner similar to the delay shown by the E1 transition of Ac^{227}.

An anthracene crystal was used for the detection of beta particles and a sodium iodide crystal was used for the detection and analysis of the coincident 40-kev photons. An analysis of the delay curve showed that an upper limit of 4 mμsec could be set for the half life of the level from which this transition occurs. Thus this confirms the work of Rasmussen and Stephens,[27] who reported the "prompt" nature of this E1 transition.

c. <u>Np^{237} decay</u>. Engelkemeir and Magnusson[19] reported the existence of a 37-mμsec metastable state following the alpha decay of Np^{237}. Stephens[18] has shown the existence of E1 transitions of energies 30 and 87 kev. The study reported herein was undertaken to see if either or both of these E1 transitions were delayed.

Quantities of Np^{237} of high isotopic purity were available from an (n, 2n) reaction on U^{238}. To remove the prolific radiations associated with the daughter Pa^{233}, a chemical separation was devised. The Np^{237} activity was put in solution and hydrogen chloride gas was passed through the solution until it was saturated with hydrogen chloride. This solution was placed on a column consisting of Dowex A-1 anion resin. (Under these conditions both neptunium and protactinium are adsorbed onto the resin.) Elution

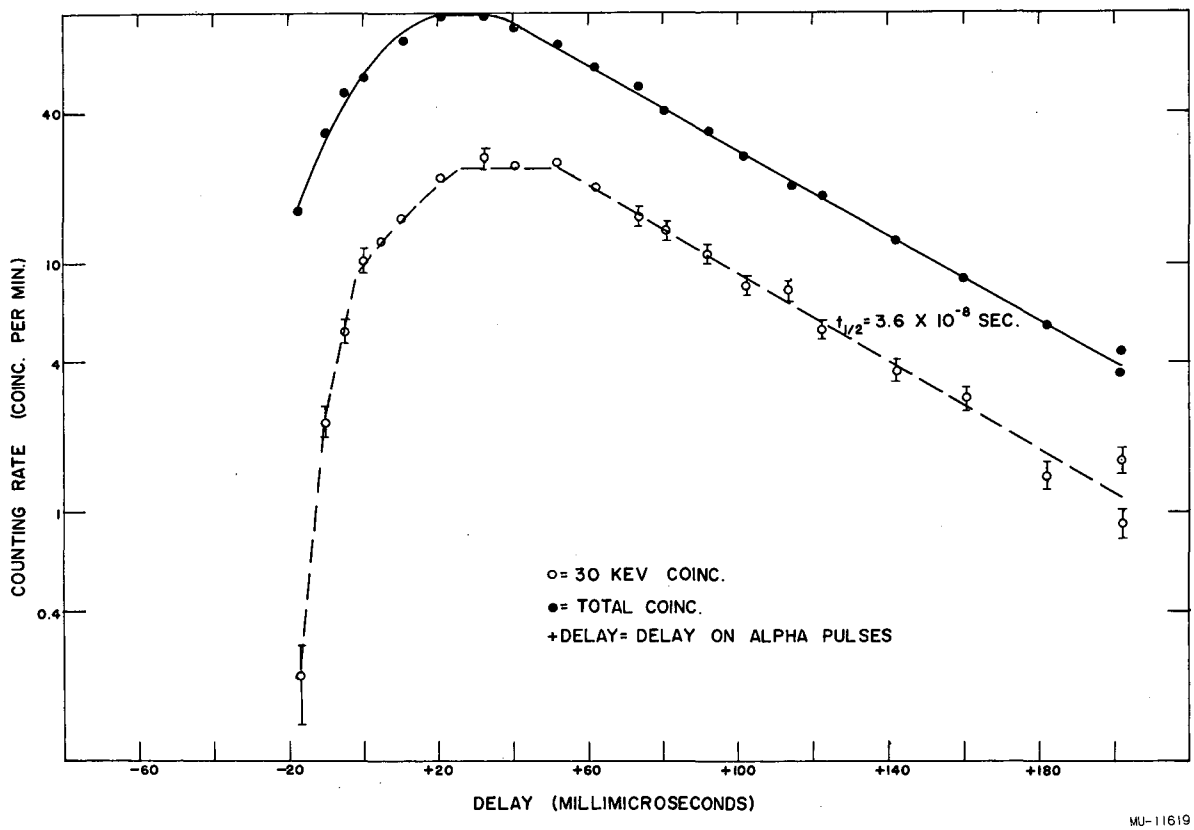

Fig. I-4 Delay Curve of 30-kev El Transition Following Np^{237} Alpha Decay

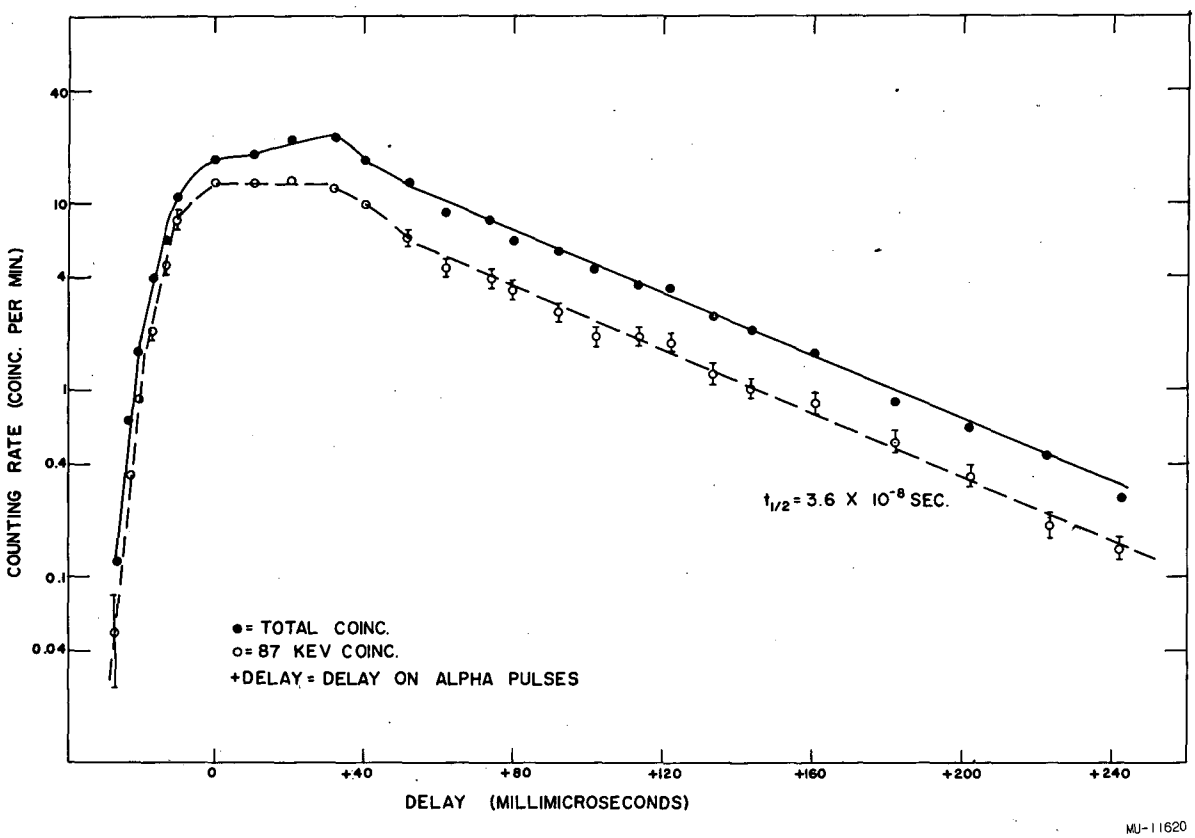

Fig. I-5 Delay Curve of 87-kev E1 Transition Following Np^{237} Alpha Decay

was then effected with dilute hydrogen chloride (1 M) which was found to remove the neptunium quickly while leaving most of the protactinium on the column. The hydrogen chloride concentration of the solution was then adjusted to 1.5 M, from which the neptunium was extracted into a 0.4 M solution of TTA in benzene. The neptunium activity was then back-extracted into an aqueous 8 M HNO_3 solution. The activity could then be mounted directly onto thin aluminum plates.

A stilbene crystal was used for the detection of alpha particles and a sodium iodide crystal was employed for the detection and analysis of electromagnetic radiations. Figures 4 and 5 are delay curves of the two photons. These two figures also show the gross coincident electromagnetic spectrum as a function of delay. These graphs clearly indicate that both the 30- and the 87-kev transitions are delayed with a half-life equal to 36 ± 4 mμsec. Careful analysis of the 87-kev photon delay curve indicates the presence of a "prompt" component with an intensity of about 25 percent of the total 87-kev photopeak. This could be attributed to K x-rays arising from the K conversion of higher-energy transitions in the decay of Np^{237}. Engelkemeir[26] has confirmed that both of the E1 transitions are delayed.

Two higher-energy photons of energies 143 and 198 kev have also been observed in the gamma spectrum of Np^{237}. A delay curve was run on these two particular gamma transitions and they appeared to be prompt. An upper limit of 2 mμsec was set for the half-lives of both transitions.

d. Th^{231} decay. Th^{231} beta-decays[22] with a 25.6-hr half-life to Pa^{231}. Beta emitter Th^{231} has been studied extensively by Freedman et al.[28] and by Stephens.[18] The decay is quite complex, and no wholly satisfactory decay scheme has yet been established. Stephens[18] has observed 26- and 85-kev transitions in this decay and has assigned them as E1 on the basis of total conversion coefficients. Pa^{233} (the daughter nucleus of Np^{237}) has E1 transitions of just about the same energies, which arise from a state with a measurable lifetime. Thus this study was undertaken to see if the analogous E1 transitions of Pa^{231} were also delayed.

A sample of U^{235} was obtained which had been isotopically enriched to a purity of more than 99 percent. This uranium activity was placed on a Dowex A-1 anion resin column. Th^{231} activity was stripped off the column by concentrated hydrogen chloride, which left the uranium on the column. The pH of the eluant was adjusted to about 4.0 and the thorium activity extracted into a 0.4 M TTA solution in benzene. The activity was back-extracted into 8 M HNO_3 and transferred to a thin aluminum plate. To check the purity of samples prepared in this manner the decay of Th^{231} was usually followed for several half-lives, during which time no deviations from a simple exponential decay were ever observed.

An anthracene crystal was used to detect the beta particles and a sodium iodide crystal was employed to detect and analyze the coincident electromagnetic radiation. Figure 6 shows the delay curve of the 26-kev photon. A similar delay curve was obtained for the 85-kev photon. Thus both E1 transitions were delayed with respect to the beta particles. To verify that this delay was not being introduced by some faulty electronic equipment, a delay curve of the "prompt" E1 transition of Ra^{225} was also run. This delay curve is also shown in Fig. 6. Figure 7 indicates the results of another run. This time the statistics were much better and only that part of the delay curve that determines the half-life is shown. The average of several of these delay curves gives a value of 41 ± 4 mμsec for the half-life of the level in Pa^{231} giving rise to these E1 transitions.

From these delay curves it appears that almost all of the radiation is delayed. However, Freedman et al.[28] have reported an intense soft beta group with an end point at 94 kev, and it is possible that the pulses from the soft betas were not of sufficient energy to trigger the coincidence circuits. In addition to these intense E1 photons there are some higher-energy gamma transitions in very low abundance. The abundance is so low that no energy determination was attempted. However, it was possible to show that most of this radiation was "prompt," with the upper limit for the half-life of the levels from which they emanate about 3 mμsec.

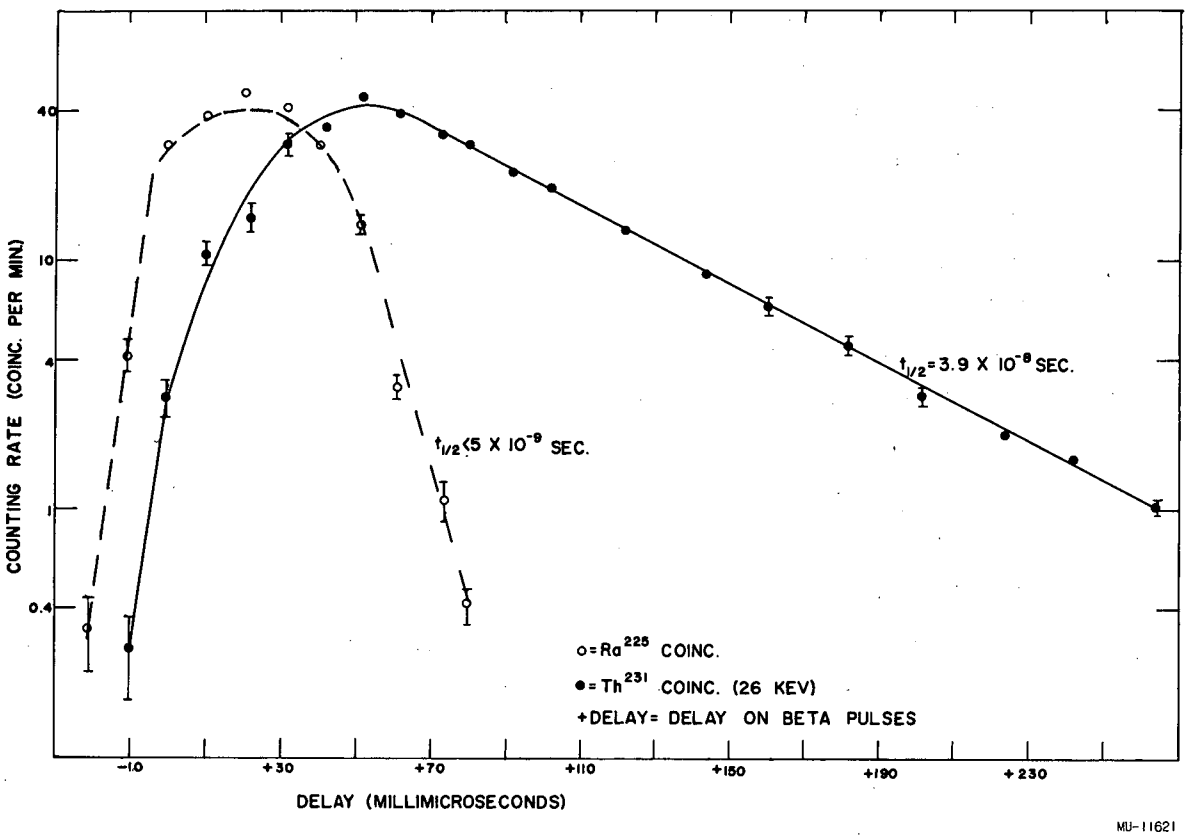

Fig. I-6 Delay Curve of 26-kev El Photon Following Th^{231} Beta Decay (with Ra^{225} Comparison Delay Curve)

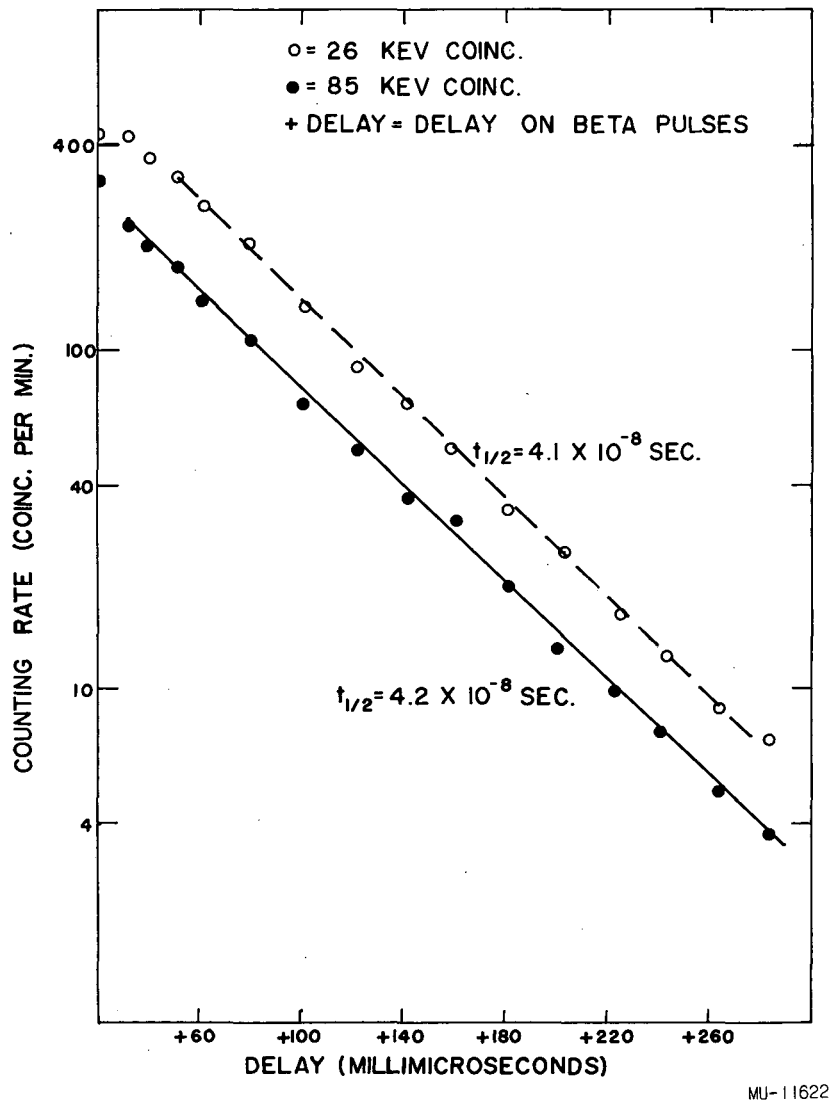

Fig. I-7 Delay Curve of El Photon Following Th^{231} Beta Decay

In addition to beta-gamma some gamma-gamma coincidences were also undertaken, using two sodium iodide crystals. The single-channel pulse-height analyzer was set to accept only electromagnetic radiation of energy about 85 kev. The 26- and 85-kev photons, along with some low-intensity higher-energy radiation, appeared in coincidence on the 50-channel pulse-height analyzer. The coincident 85-kev photopeak appeared too broad to be due to a single gamma ray. A long delay (about 80 mμsec) was put on the gate pulses leading into the fast-coincidence circuit. (Under these conditions the coincidence spectrum shows the gamma rays delayed with respect to K x-rays.) The coincidence spectrum showed the 26- and 85-kev photons, but the higher-energy radiation was no longer present. The 85-kev photopeak in this spectrum no longer appeared complex. It also appeared to be a little lower in energy than the prompt-coincidence peak.

A long delay (about 80 mμsec) was placed on the signal pulses leading into the fast-coincidence circuit. Under these conditions the coincidence spectra show those gamma rays which populate the metastable state. The peak at 26 kev disappeared but the photopeak at about 85 kev remained in the spectrum. The peak appeared complex and displaced towards a little higher energy than the prompt-coincidence peak. In addition this spectrum showed some higher-energy radiation in low abundance.

Thus, we conclude that all gamma transitions of energy greater than 85 kev emanate from states above the metastable level and that at least one of these higher-energy transitions populates the metastable level.

Stephens[18] has already reported one discrepancy in the decay scheme proposed by Freedman et al.[28] The above data are contrary to another phase of that proposed decay scheme. According to that decay scheme about 50 percent of the 26-kev photons should be prompt, since Freedman et al.[28] have postulated a relative hard beta group populating a 26-kev level directly. The delay curves of the beta-26-kev photon coincidences do not show any prompt component (at least 90 percent of the 26-kev photons are delayed).

This discrepancy cannot be explained by the soft beta group, since the beta group populating the 26-kev level would be relatively hard in Freedman's decay scheme.

Recently, Hoff and Mann[29] have studied the alpha decay of Np^{235}, which decays to the same daughter nucleus, Pa^{231}. Their work has confirmed the existence of a metastable state with a half life of about 40 mμsec.

e. Cf^{249} decay. Cf^{249} is an alpha emitter with a half life of 400 to 500 yr.[30] It may be prepared by intensive neutron irradiation of lower elements.[30] The samples used in this study were milked from a separated berkelium fraction, to reduce the amounts of Cf^{250}-Cf^{252} present, and then mounted on a 0.00025-in. platinum plate. Stephens[18] has studied this isotope and has proposed a tentative decay scheme. The main gamma transition has an energy of 394 kev, with weaker transitions at 341 and 270 kev. The 341- and 394-kev transitions have been assigned as probably E1 on the basis of K-conversion coefficients.[31] The photon of energy about 270 kev has not been assigned a multipolarity.

Figure 8 shows the delay curves of the two high-energy gamma rays. A stilbene crystal was used to detect alpha particles, and a sodium iodide crystal was used to detect and analyze electromagnetic radiations. From the delay curves we may set an upper limit of 0.8 mμsec for the half life of the levels from which these transitions occur.

f. Th^{227} decay. Th^{227} alpha-decays[22] with a 19-hr half life to Ra^{223}. Hyde[32] has reported the existence of a 50-kev transition whose total conversion is so low that the transition can only be E1. There is another intense transition, of energy 236.1 kev, which has been assigned as E1 by Pilger[33] on the basis of K and L conversion coefficients.

A sample of this activity was made available and a delayed-coincidence experiment was carried out to see if either or both of these transitions have measurable lifetimes. A potassium iodide crystal was used to detect and analyze alpha particles, and a sodium iodide crystal was employed to analyze the coincident electromagnetic spectrum. Electromagnetic radiation peaks were seen at 50, 80, and

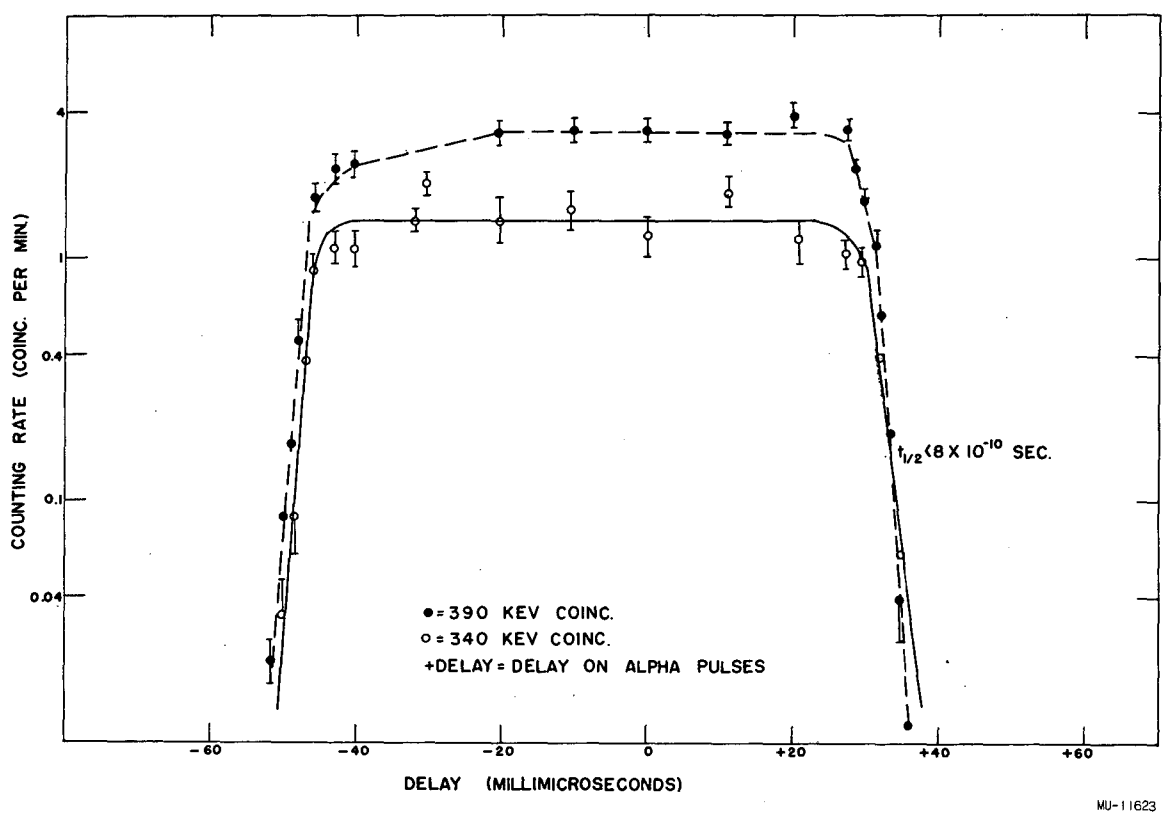

Fig. I-8 Delay Curves of Gamma Rays Accompanying Cf^{249} Alpha Decay

235 kev. The latter peak was much too broad to be due to a single gamma ray.

The delay curves were analyzed and all photons appeared to be "prompt." An upper limit of 2 mμsec could be set for the half life of the 50-kev E1 transition and an upper limit of 1 mμsec could be set for the half life of the 236-kev transition. The K x-rays also appeared to be prompt with respect to the initial alpha particles. This, in part, confirms the work of Rasmussen and Hyde[34] who previously observed the prompt nature of the 50-kev E1 transition.

g. U^{235} decay. Stephens[18] has studied the alpha decay of U^{235} in considerable detail and has proposed a decay scheme. The main gamma transitions accompanying the decay have energies of 184, 143, and 109 kev. All three of these transitions have been assigned as E1 on the basis of K-conversion coefficients.[18]

The U^{235} sample described in the section on Th^{231} decay was available for this study. No attempt was made to chemically remove the Th^{231} daughter, as it grows into the U^{235} sample too rapidly to be practical. As Th^{231} is a beta emitter it in no way interfered with the alpha-gamma coincidence experiments. A stilbene crystal was used to detect alpha particles, and a sodium iodide crystal was used for the detection and analysis of gamma radiation.

The specific activity of U^{235} is too low to permit good statistics to be obtained on delay curves. However, one delay curve was run between alpha particles and the most intense gamma ray, the 184-kev photon. This run permits us to set an upper limit of 1.5 mμsec for the half life of the state from which this transition emanates. In the decay scheme proposed by Stephens[18] all three E1 transitions depopulate the same level. Therefore this half-life limit will be true for all three E1 transitions in the U^{235} decay.

h. Tl^{209} decay. Tl^{209} is a 2.2-min beta emitter,[18, 22, 35, 36] which may be prepared from the natural radioactive product Th^{229}. Due to the short half life of Tl^{209} it is not practical to isolate this activity. Instead, a sample of Ac^{225} was chemically separated from its Th^{229} parent and the Tl^{209} activity studied was in transient equilibrium with the Ac^{225} parent. Thus this sample contained all

the other activities that are in the Ac^{225} decay chain. However, there are only three beta emitters in this chain. One, Pb^{209}, has a 0.64-Mev beta group with no gamma transitions following the beta decay. Bi^{213} has two beta groups, one with an end point at 1.39 Mev and the other at 0.959 Mev. There is also a 434-kev gamma ray present in the Bi^{213} decay scheme. Thus, only this 434-kev photon can interfere with the beta-gamma coincidence measurements made on Tl^{209}.

Tl^{209} has a beta end-point energy of 1.99 Mev, and its decay scheme has been studied (see Fig. 9).[18] In this disintegration scheme there are three transitions, of energies 120, 450, and 1560 kev, in cascade. The 120-kev transition has been assigned as E1 on the basis of K- and L-conversion coefficients.[18, 35]

A lucite disc impregnated with terphenyl was used for the detection and analysis of beta particles. Scotch tape was placed over the side of the disc facing the Ac^{225} sample so that alpha particles would not trigger the "gate." A sodium iodide crystal was used for the detection and analysis of the coincident radiation. The single-channel pulse-height analyzer was set to count all beta particles above the photomultiplier noise level.

Beta-gamma coincidences showed coincident gamma radiation at 120, 450, and 1560 kev, and in addition a peak at 80 kev due to K x-rays. The peak at 450 kev is actually a composite of the 434-kev gamma ray from Bi^{213} beta decay and the 450-kev gamma ray from Tl^{209} beta decay.[18, 35] The Bi^{213} 434-kev gamma ray is approximately 20 times as intense as the 450-kev gamma ray of Tl^{209} in this sample. This results from the fact that Bi^{213} decays primarily by beta emission and the level of the Tl^{209} activity is determined by the alpha branching ratio of Bi^{213}, which is of the order of 2 percent.

Figure 10 shows the delay curves of the K x-rays and 120-kev gamma transitions. Careful analysis of the K x-ray delay curve shows a prompt component and then a delayed component. The 120-kev delay curve shows only one delayed component. Figure 11 shows the low-energy coincident electromagnetic radiation in both

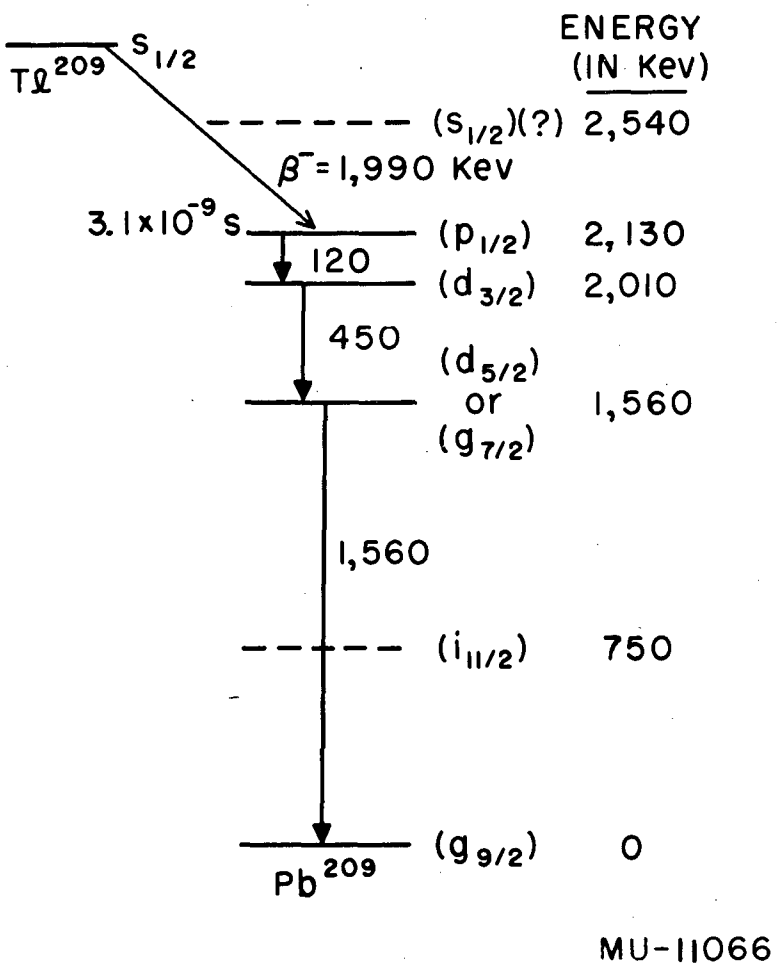

Fig. I-9 Proposed Decay Scheme of Tl^{209}

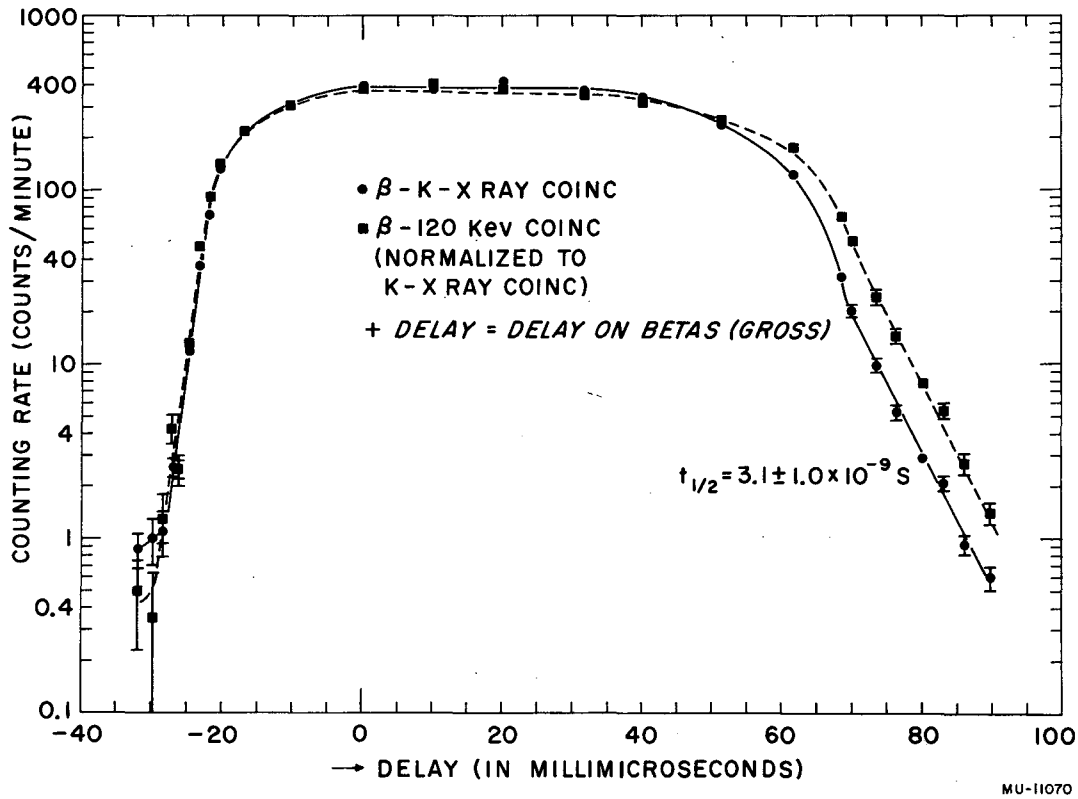

Fig. I-10 Delay Curves of K X-Rays and 120-kev Gamma Rays Following Beta Decay of Tl^{209} and Bi^{213}

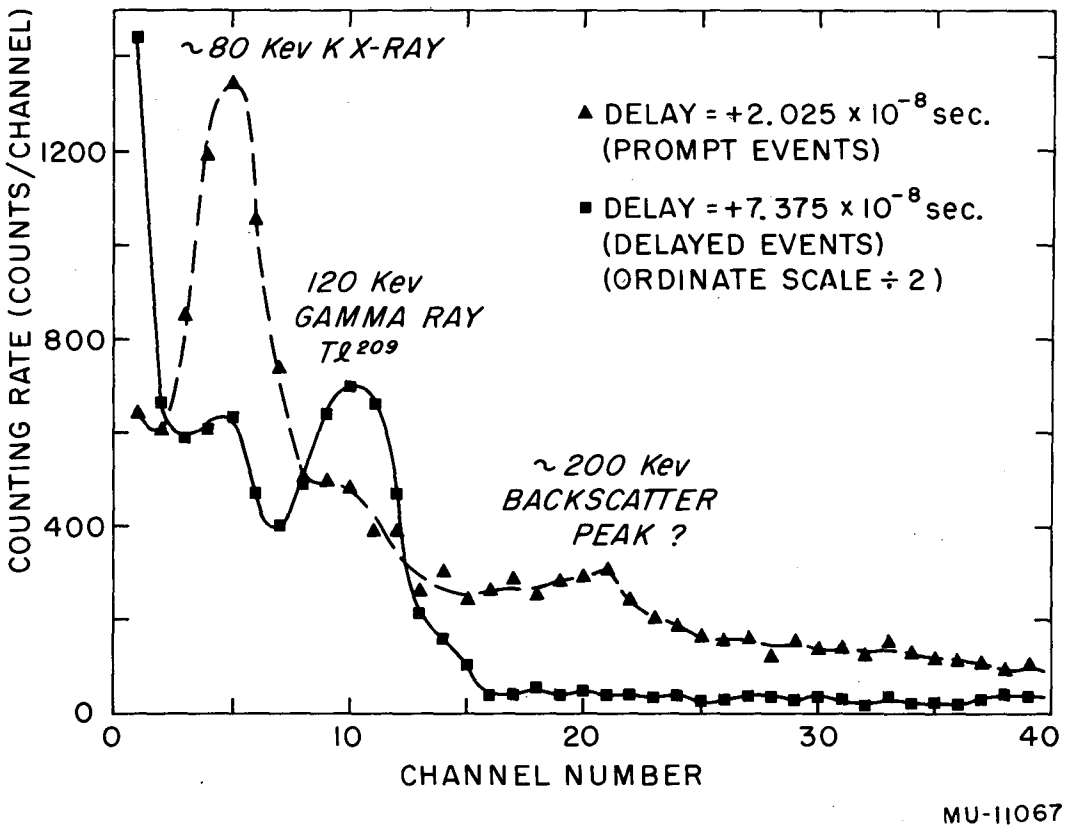

Fig. I-11 Low Energy Electromagnetic Radiation Coincident with Beta Particles of Tl^{209} and Bi^{213}

prompt and delayed coincidence. In prompt coincidence the K x-ray peak is more intense than the 120-kev photopeak, but in delayed coincidence the 120-kev photopeak is more intense than the K x-ray peak.

Let us consider two electromagnetic radiations gated by the same initial event with the half-lives of both transitions short compared to the finite slope of the delay curve. Let us now consider the delay curves of the two radiations. As more and more delay is introduced on the gate pulses, the counting rates of the two photons decrease. However, the counting rate of the higher-energy radiation decreases with a smaller delay on the gate pulses than is necessary to decrease the counting rate of the lower-energy radiation by the same factor. The delay curves for Tl^{209} in Fig. 10 exhibit the opposite behavior and are evidence for a delayed transition.

Other experiments were made to further verify the existence of a metastable state. As the 450- and 1560-kev transitions are in cascade and succeed the 120-kev transition,[18] both these transitions must also be delayed with respect to the initial beta particles. The beta—450-kev gamma delay curve showed a prompt component ($t_{1/2}$ < 2 mμsec) and then a delayed component. The prompt component was thought to be the 434-kev gamma transition of Bi^{213}. To prove this the single-channel discriminator was set above the 0.96-Mev end point of the beta group populating the 434-kev level in Po^{213} but below the 1.99-Mev end point of the Tl^{209} beta spectrum. Under these conditions the beta—450-kev delay curve showed no prompt component but only a single delayed 450-kev gamma transition. Figure 12 shows the two different delay curves normalized at their peak coincidence-counting rates.

The counting efficiency of the 1560-kev photon is too low[10] to permit a direct beta—1560-kev delay curve to be run, but a delay curve integrating all gamma rays above 500 kev showed that essentially everything higher than 500 kev was delayed.

The half-life of this metastable state as determined from the average of several delay curves is 3.1 ± 1.0 mμsec.

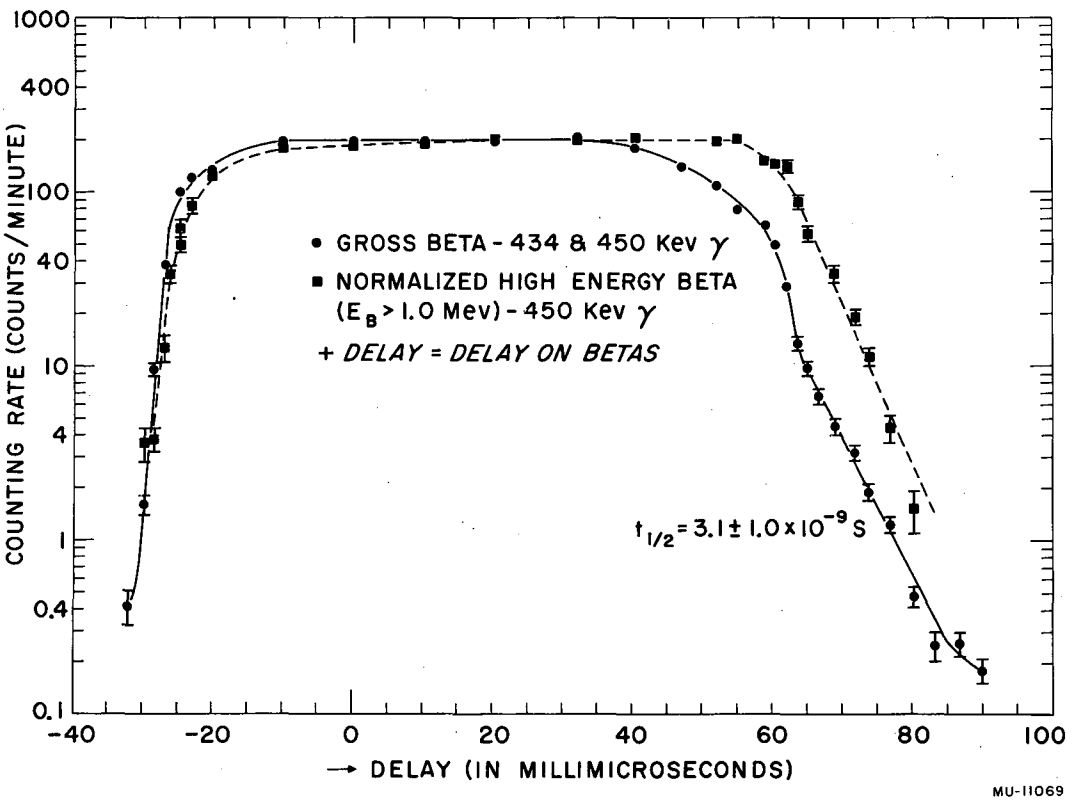

Fig. I-12 Delay Curves of 434-kev and 450-kev Gamma Rays Following Beta Decay of Tl^{209} and Bi^{213}

One gamma-gamma coincidence experiment was also performed. The single-channel analyzer was set on the 120-kev photon, and delay curves were run for the coincident 450- and 1560-kev gamma rays. The results of this experiment enable us to set an upper limit of 1.5 mμsec for the half-lives of both transitions.

i. U^{230} family decay. Another group of E1 transitions studied were those emanating from the 1- states of even-even nuclei.[18] Low-lying 1- states have been well established in that part of the periodic table around 136 neutrons. The 1- states usually decay by E1 transitions to the 0+ ground state and the 2+ first excited state. The assignment of E1 multipolarity to these transitions has been made chiefly on the basis of alpha-gamma angular correlation experiments. It is convenient to study these low-lying 1- states in the U^{230} decay chain. The activities of main interest are alpha emitter U^{230} itself and 31-min alpha emitter Th^{226}, the immediate daughter of U^{230}.

A sample of U^{230} was made by bombarding thorium metal with high-energy protons. The target was allowed to stand about a month to give the Pa^{230} formed time to decay into U^{230}. At the end of this period chemical separation of the uranium yielded essentially pure 20.8-day U^{230}, into which its daughters soon grew. This sample was transferred to a thin aluminum plate.

A stilbene crystal was used for the detection of alpha particles and a sodium iodide crystal was employed for the detection and analysis of the coincident electromagnetic spectrum. The coincidence spectrum is complex, but previous work[18] had identified three E1 transitions which could be seen in the spectrum. There was a peak at about 240 kev which contained an E1 transition of energy 230 kev from U^{230} decay and an E1 transition of energy 240 kev from Th^{226} decay. These two gamma rays could not be resolved from each other but the composite peak was somewhat wider than a photopeak due to a single photon should be. On this justification it was assumed that both transitions were present in the spectrum. The third E1 transition observed was the 160-kev photon emanating from the 1- level of Th^{226} following alpha decay of U^{230}.

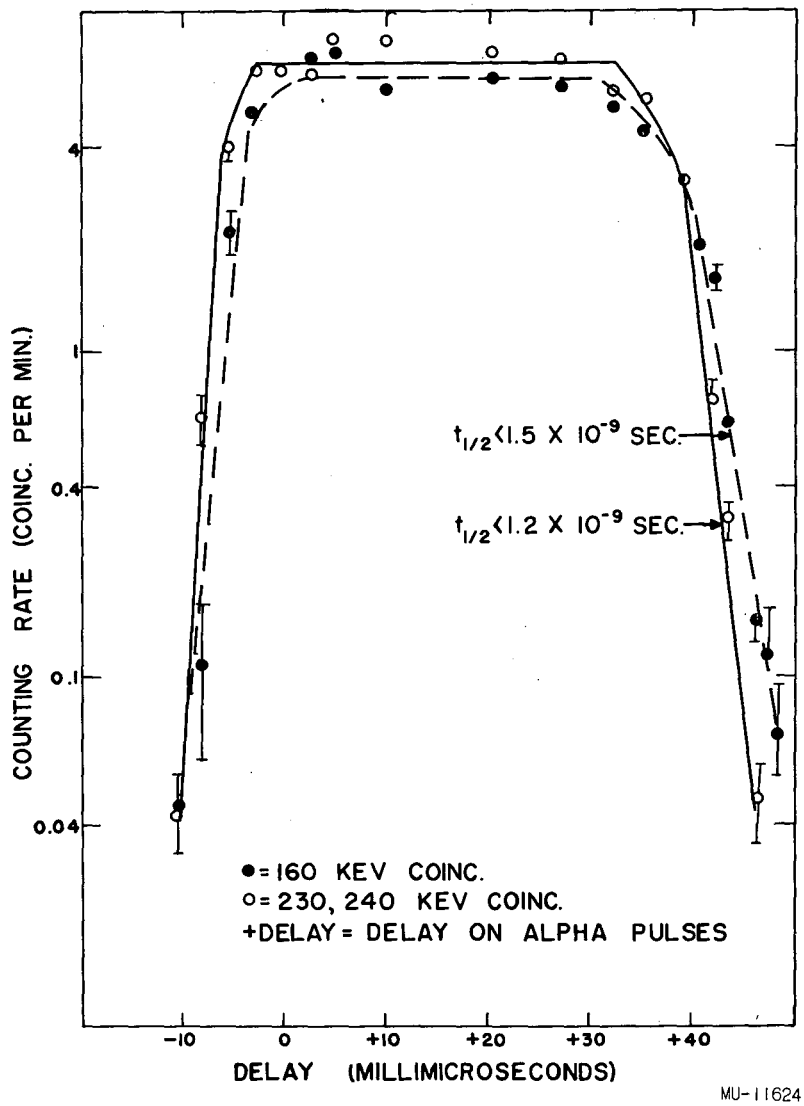

Fig. I-13 Delay Curves of El Photons Present in U^{230} Family Decay

Figure 13 shows the delay curves of both the 160-kev and the combined 240-kev gamma rays. The results of these delay curves enable us to set an upper limit of 1.2 mμsec for the half life of the two photons in the 240-kev peak. Likewise an upper limit of 1.5 mμsec may be set for the half life of the 160-kev transition. Thus we can set an upper limit of 1.2 mμsec for the half lives of the 1-levels in both Th^{226} and Ra^{222}.

2. Magnetic Dipole Transitions

The lifetimes of M1 transitions seem to vary erratically in somewhat the same manner as E1 transition probabilities.[4] However, in general, most M1 transitions proceed too rapidly to measure their transition probabilities easily by the method of delayed coincidences. Nevertheless, the studies described here were undertaken to determine if there were any delayed M1 transitions in the heavy region.

a. Cm^{243} decay. Cm^{243} decays to Pu^{239} by alpha emission with a half life of about 35 years.[31] Np^{239} beta-decays to the same daughter nucleus. Graham and Bell[37] reported the existence of a 1.1-mμsec in Pu^{239} following the beta decay of Np^{239}. They observed that the beta coincidence counting rates of the 210-, 227-, and 276-kev transitions all followed the 1.1-mμsec half life. The multipolarity of these transitions has been established as principally M1[38] on the basis of relative K- and L-subshell and absolute K-conversion coefficients. It was therefore decided to reinvestigate the delayed nature of these M1 transitions.

This study was carried out from the Cm^{243} alpha decay because of the more convenient half life. A sample of Cm^{243} was chemically separated from a quantity of Pu^{239} which had undergone extensive neutron bombardment. By alpha activity this sample was approximately 90 percent Cm^{242}, but this activity did not interfere with the measurements.

A stilbene crystal was used for the detection of alpha particles and a sodium iodide crystal was used for the detection and analysis of electromagnetic radiation. Figure 14 shows the delay curve of the 278-kev photon. For comparison purposes we have dotted in a line

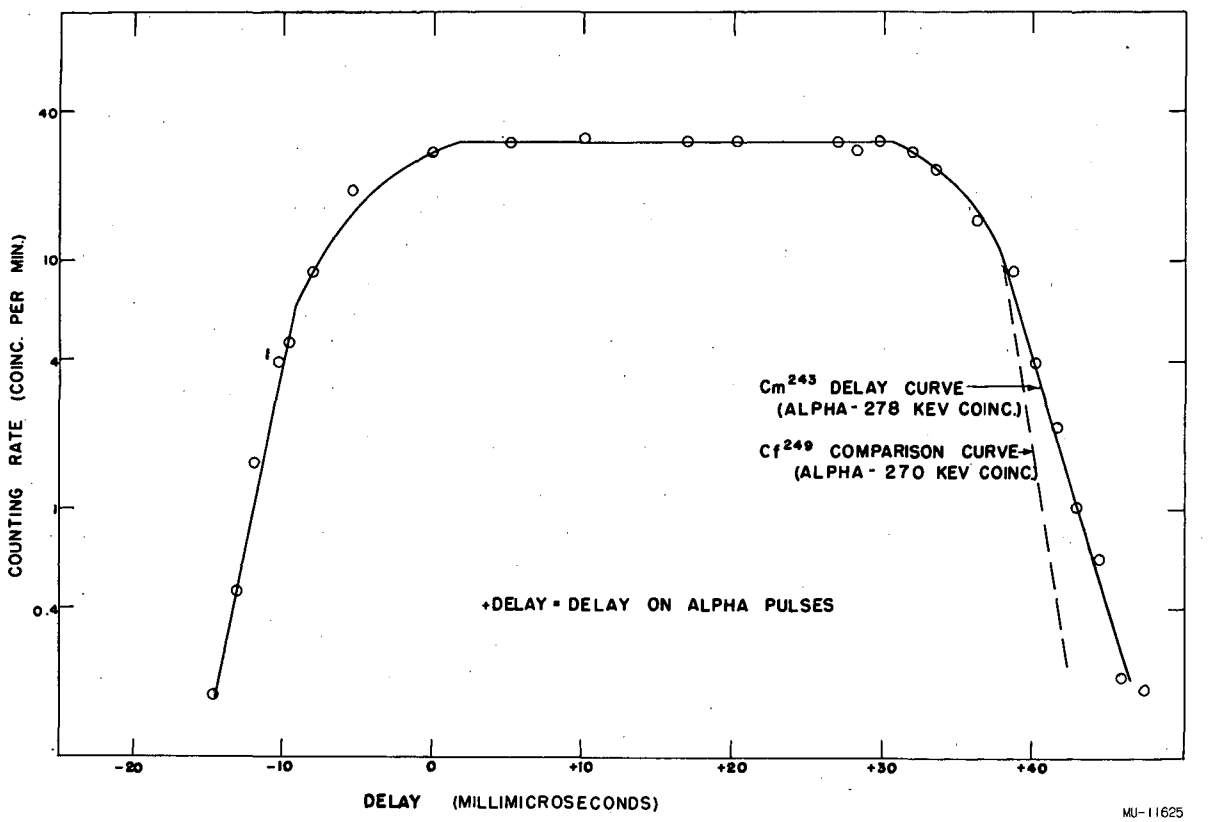

Fig. I-14 Delay Curve of 278-kev Photon Following Cm^{243} Decay

obtained experimentally from a Cf^{249} delay curve described previously. This graph clearly shows that the 278-kev transition is delayed with respect to alpha-particle emission.

An analysis of this delay curve similar to the analysis suggested by Newton[15] yielded a value of about 1.2 mμsec for the half life of the level from which these M1 transitions emanate.

b. Bi^{213} decay. It has already been noted under the decay of Tl^{209} that a 434-kev transition following beta decay of Bi^{213} was "prompt" ($t_{1/2} < 2$ mμsec). Stephens[18] has assigned this transition as M1.

c. Re^{183} decay. Re^{183} decays by electron capture to W^{183}. Previous work[39] has indicated that prolific radiations are associated with this decay. The most intense radiations associated with the decay are three transitions of energy about 160 kev--two of which are assigned as M1 transitions--and two transitions of energy around 100 kev--one of which is assigned as an M1 transition. All of these multipolarity assignments were made on the basis of relative K-and L-subshell conversion coefficients.[40]

A sample of Re^{183} was chemically separated from a tantalum target that had been bombarded with 40-Mev alpha particles. The single-channel analyzer was set on the K x-ray photopeak. Delay curves were then run, and an upper limit of 4 mμsec could be set for the half lives of all the above transitions.

d. Pa^{231} decay. Following the alpha decay of Pa^{231} there is a 300-kev transition assigned as M1.[41] An upper limit of 1.5 mμsec was set for the half life of this transition.

3. Electric Quadrupole Transitions

The study of E2 transition probabilities is of much interest, as the Bohr-Mottelson theory[6] predicts that certain E2 transitions will proceed at a more rapid rate than would be expected for a single-particle transition. Accordingly several studies of E2 transition lifetimes were undertaken. Some work on the disintegration scheme of Re^{184} is also discussed in this section.

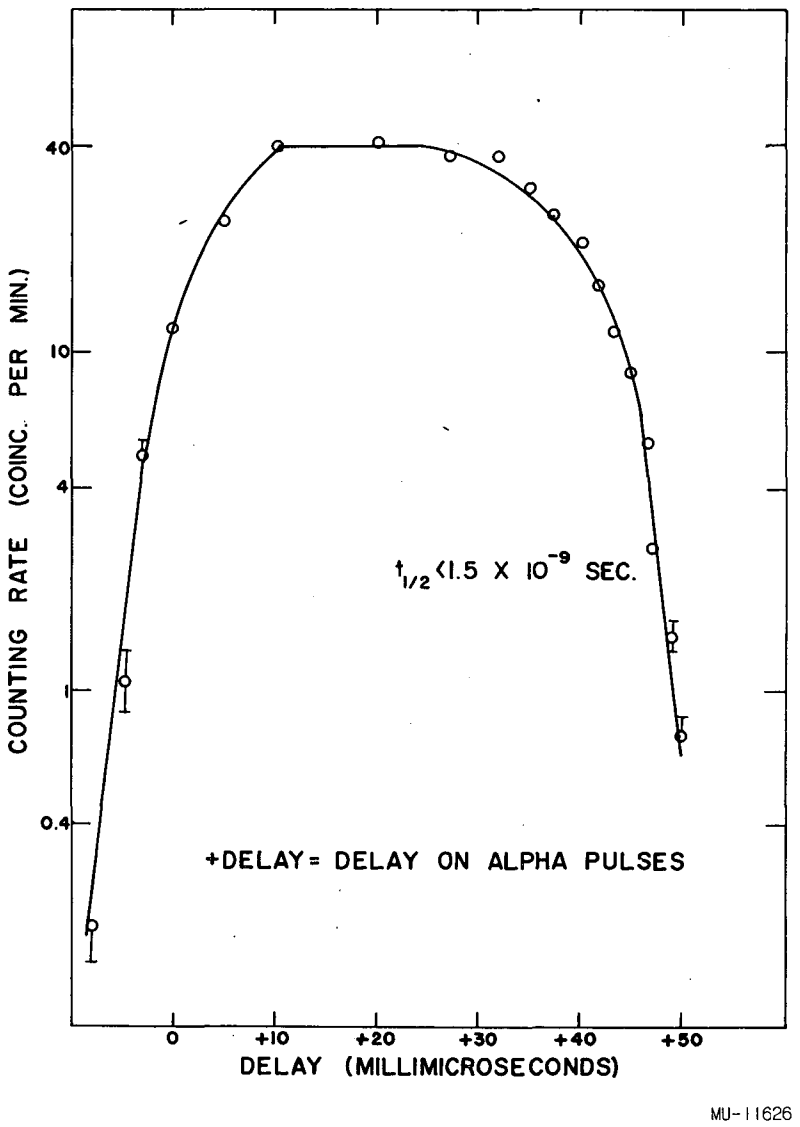

Fig. I-15 Delay Curve of E2 Transition Present in U^{230} Family Decay

a. U^{230} family decay. Some aspects of the U^{230} family decay have already been discussed in the section on E1 transitions. The experimental conditions described in that section are identical to those used for these studies. In the U^{230} family the following E2 transitions are present:[18] a 70-kev transition following the alpha decay of U^{230}, 110- and 190-kev transitions following the alpha decay of Th^{226}, and a 330-kev transition following the alpha decay of Ra^{222}. The multipolarity assignments were made on the basis of conversion coefficients and alpha-gamma angular correlation experiments.

Figure 15 shows one of four delay curves obtained in this study. All of the transitions appeared "prompt," with the following upper limits set from the delay curves: 330-kev transition, $t_{1/2} < 0.8$ mμsec; 70- and 190-kev transitions, $t_{1/2} < 1.5$ mμsec; 110-kev transition, $t_{1/2} < 1.4$ mμsec.

b. Re^{184} decay. Re^{184} decays by electron capture to W^{184} with a 50-day half-life.[22, 42] Previous work[43, 44] has shown that the first excited state has a spin of 2+ and that this state de-excites by an E2 transition of energy about 112 kev. Several other transitions have also been reported accompanying Re^{184} decay.[42] A sample of Re^{184} was chemically separated from a tantalum target that had been bombarded with 40-Mev alpha particles. A permanent-magnet electron spectrograph[45] was used to accurately determine the energy of the first excited state as 111.2 kev. Not enough activity was made to see any other electron lines that could be attributed to Re^{184} decay.

Gamma photopeaks at energies 780 and 890 kev were seen on a sodium iodide scintillation counter. The relative intensities of these two photons are as 67:100. The decay of these two transitions was followed for three half-lives and showed no deviation from a simple exponential decay. The photons decayed with a half-life equal to 52 ± 10 days. Unfortunately the rhenium sample prepared in the above manner contained a large proportion of Re^{183}. Re^{183} decay is accompanied by prolific low-energy radiation[39] which completely obscured the low-energy part of the Re^{184} gamma spectrum.

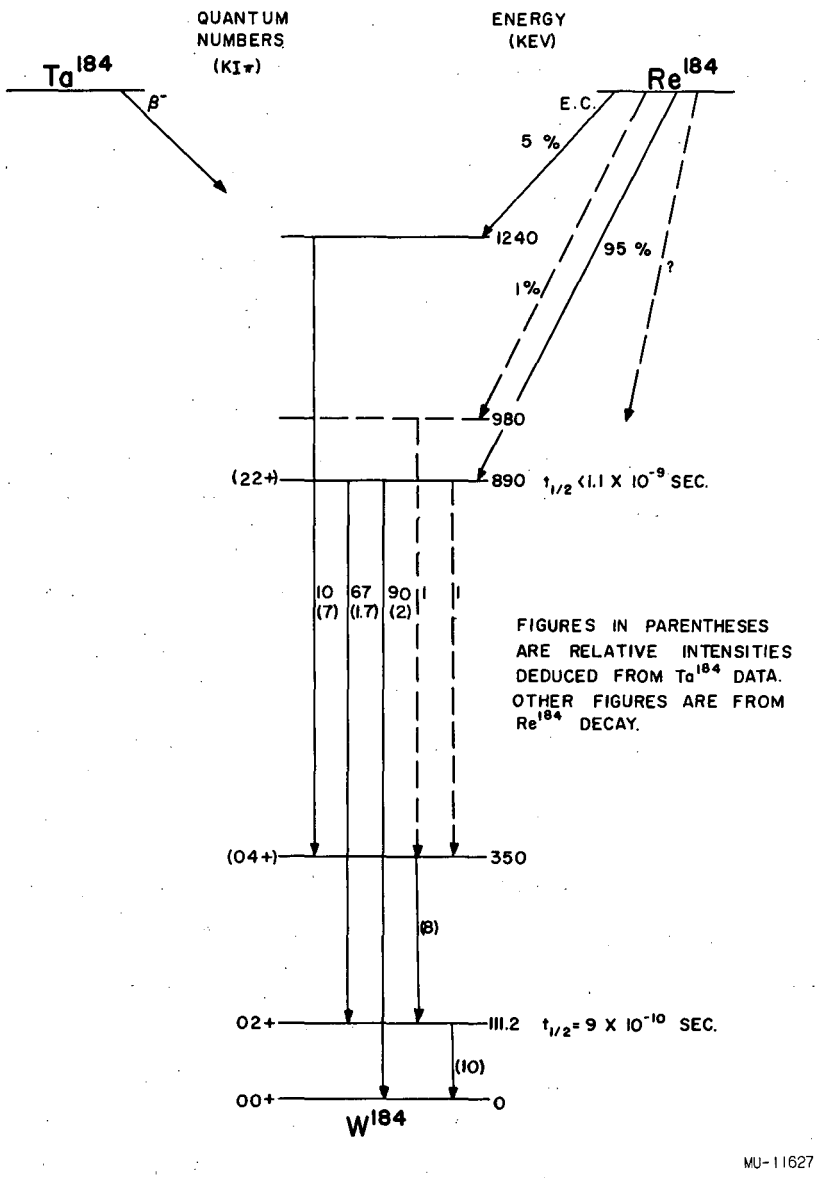

Fig. I-16 Proposed Decay Scheme of Re^{184}

Gamma-gamma coincidences were run on Re^{184} in an attempt to clear up the decay scheme. K x-rays (~120 percent) and 110-kev photons (~35 percent) were seen in coincidence with the 780-kev photon. K x-rays (~100 percent), 110-kev photons (~3 percent), and 240-kev photons (~8 percent) were seen in coincidence with the 890-kev photons. In addition, low-intensity coincidences were seen between 240-kev photons with both 540- and 630-kev gamma rays. To make sure that these two coincidences were not due to the higher-energy photons scattering off one sodium iodide crystal into the other, the two scintillation counters were set up in such a manner that they could not "see" each other. This experiment gave positive results. However, the poor coincidence geometry coupled with the low intensity of the two photons resulted in very poor statistics, and the existence of the 540- and 630-kev gamma rays is somewhat doubtful. The intensity of both the 540- and 630-kev gamma rays is estimated to be 1 percent of the 890-kev photon intensity.

In constructing a decay scheme we first note that most of the 890-kev photons are in coincidence with only K x-rays. Therefore it seems reasonable that there is a level at 890 kev which depopulates at least in part by an 890-kev transition to the ground state. It is known that the first excited state has an energy of 110 kev and that there are abundant 780--110-kev coincidences. Thus the 780-kev transition must also depopulate the 890-kev level. In even-even nuclei with a large prolate spheroidal deformation the Bohr-Mottelson theory[6] predicts the existence of a 4+ level at an energy 3.33 times the energy of the 2+ state. Therefore this theory predicts a level at about 365 kev. However, at mass number 184 nuclei are not as deformed as they are at lower mass numbers, where the Bohr-Mottelson unified model[6] holds more accurately. Therefore we would expect the 4+ level to be somewhat depressed in energy and it is reasonable to place the 240-kev transition as a 4+ to 2+ transition. The three transitions seen in coincidence with the 240-kev photon may then be placed directly populating the 4+ level. This proposed decay scheme for Re^{184} is shown in Fig. 16.

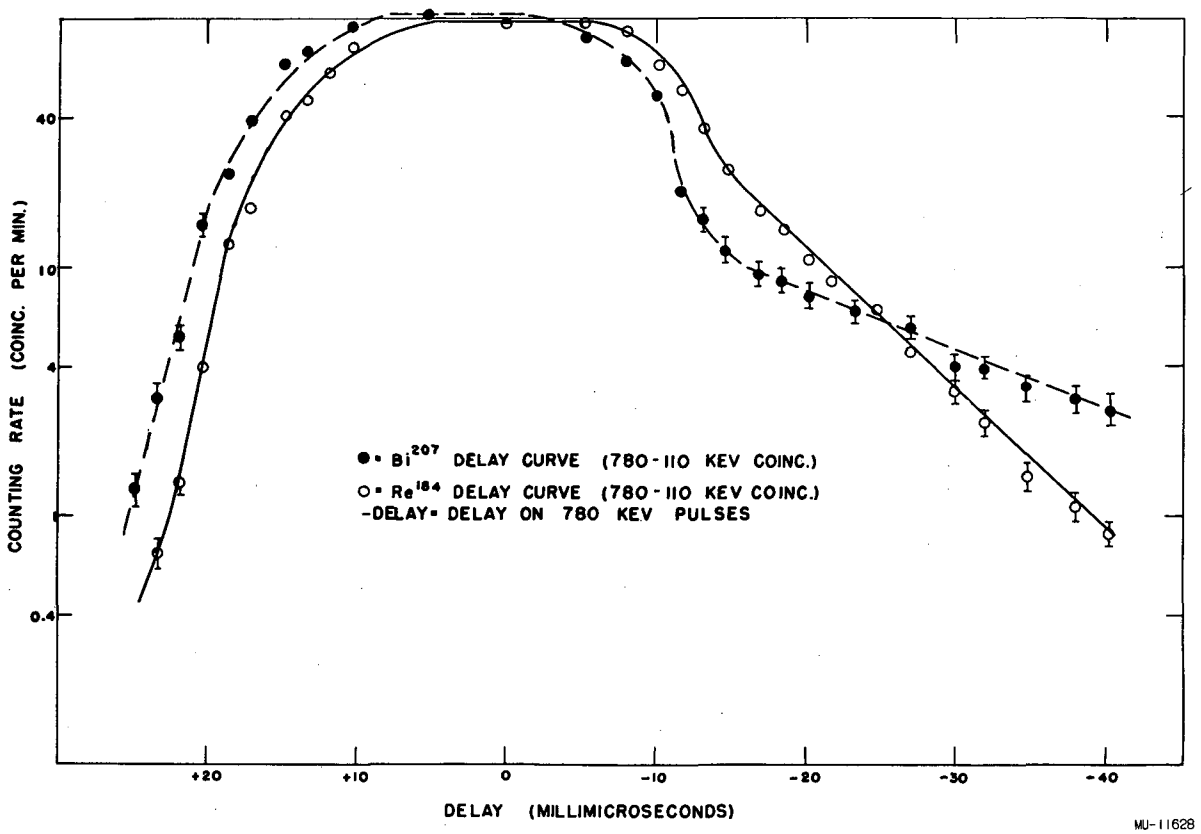

Fig. I-17 Delay Curve of 780 - 110 kev Coincidences Following Re^{184} Decay Compared with Bi^{207} Delay Curve

By gating on K x-rays we were able to set an upper limit for the half-life of the 890-kev level at 1.1 mμsec. In another experiment a delay curve was run between 780- and 110-kev photons. This delay curve is compared with one taken of Bi^{207} in Fig. 17. For the purposes of this comparison the single-channel pulse-height analyzer in the Bi^{207} run was set to accept the same energy range as for the Re^{184} run, and the same channels on the 50-channel pulse-height analyzer were integrated in both cases. From this direct comparison we can see that the 110-kev level is a metastable state. The centroid-shift method suggested by Bay[14] was used to obtain the half-life of the 110-kev level. Thus, the half-life was found to be $9 \pm 3 \times 10^{-10}$ sec.

It is interesting to compare the results of the electron-capture decay of Re^{184} to W^{184} with some data[46] obtained from the beta decay of Ta^{184} to the same nucleus. In the beta decay, photons were reported at energies of 110, 160, 210, 240, 300, 405, 780, 890, and 1180 kev with relative intensities 3, 1, 1, 6, 3.5, 10, 1.7, 9, and 5. The increased intensity of the 890-kev photon relative to the 780-kev gamma ray indicates that the 1240-kev level is more heavily populated in the beta decay. It is also interesting to note that when we correct the 110- and 240-kev transitions for internal conversion we obtain a rough intensity check of the various transitions. The total conversion coefficient of the 240-kev transition is estimated at 0.25 from Rose's tables,[47] while the total conversion coefficient of the 110-kev transition is taken to be 2.0 from the above data on 780-110-kev coincidences. Figure 16 shows the rough intensity check from Ta^{184} decay.

The 160-kev photon observed in Ta^{184} decay is probably not real, but due to backscattered higher-energy gamma rays. However, the other four photons are not seen in Re^{184} electron-capture decay and Ta^{184} must populate some levels not populated by Re^{184} decay.

c. <u>Fr^{221} decay</u>. The 4.8-min alpha emitter Fr^{221} is another activity present in the Ac^{225} decay chain previously discussed in the section on Tl^{209} decay. Accompanying the alpha decay there is a 220-kev transition, which has been assigned as E2.[18] An upper limit of 1 mμsec was set for the half-life of this transition.

d. Other results. Table I gives a list of nuclides that have been studied but were not discussed in the previous sections. In all of these cases, no appreciable number of delayed coincidences were observed above the expected random rate. Specific limits were set only for those photons clearly in the gamma spectra. In all these cases the existence of long-lived isomers (half life > 1 μsec) is possible.

Table I

Data for Various Transitions in Heavy Region

Parent Nuclide	Half-life	Daughter Nuclide	Energy of Gamma (kev)	Multipolarity of Gamma	Half-life of Gamma (mμsec)
Po^{206}	9 d	Bi^{206}	1031	E1	< 2
			806	E2	< 2
			511	M1	< 2
			522	M1	< 2
			586	M1	< 2
Po^{207}	5.7 h	Bi^{207}	992	M1 + (E2)	< 4
			742	M1 + (E2)	< 5
			405	M1 + (E2)	< 5
$Po^{208,9}$	100 y	$Bi^{208,9}$	900	M1	< 1
	2.9 y		600	-	< 1
			290	-	< 1
At^{211}	7.5 h	Po^{211}	680	-	< 1.5
Gd^{149}	9 d	Eu^{149}	150	-	< 1.8
			290	-	< 1.9
			760	-	< 1.8
Ac^{225}	10 d	Fr^{221}	100	-	< 3
Bi^{205}	15 d	Pb^{205}	703	E2	< 5

D. Discussion of Results

1. Electric Dipole Transitions

The results of E1 transition lifetime measurements for odd-mass nuclides in the region of spheroidal deformed nuclei are discussed in Part II. Tl^{209} and U^{230} decay are discussed in this section.

a. Tl^{209} decay. The 120-kev E1 transition is 3.6×10^4 times slower than a simple single neutron ($p_{1/2} \xrightarrow{E1} d_{3/2}$) transition should be (cf. Eqns. VII-1 and VII-7 of Bohr and Mottelson[6]).

The delayed nature of this transition can be explained in terms of parentage overlap.[48] We can make a plausible set of spin assignments as shown in Fig. 9 from consideration of the shell model, from spins of neighboring nuclei, and from the observed gamma radiations in the Tl^{209} beta decay. The spins of Fig. 9 are slightly different from those of Harvey.[49] The level at 750 kev was seen by Harvey[49] in the (d, p) reaction on Pb^{208}, but this level is not populated in the beta decay of Tl^{209}. Note that the 1/2 level can be formed only by breaking the closed shell of 126 neutrons. This particular level, however, is more than 2 Mev above the ground state; therefore it seems reasonable to make the assignment of principal neutron configuration as $(g_{9/2})^2 (p_{1/2})^1$ plus 124 filled orbitals.

The 3/2+ level has as its principal configuration $(p_{1/2})^2 (d_{3/2})^1$ with a small admixture of $(g_{9/2})^2 (d_{3/2})^1$. The schematic representation of the nucleons involved in the E1 transition is given in Fig. 18.

It seems reasonable that the transition proceeds only by virtue of the small admixture of the neutron configuration $(g_{9/2})^2 (d_{3/2})^1$ in the final state. The large hindrance indicates a very small configuration mixing. This type of reasoning is similar to that used by Sunyar et al.[50] in explaining some features of the beta decay of Kr^{85} to Rb^{85}. In the language of fractional-parentage theory[48] we may say that the principal configurations of the 1/2- and the 3/2+ levels have no common parents.

Another interesting feature is the log ft value of 5.5 for the beta decay of Tl^{209}, which we assume to have an $s_{1/2}$ proton hole in the 82-proton structure, like Tl^{203}, Tl^{205}, and Tl^{207}. With our spin

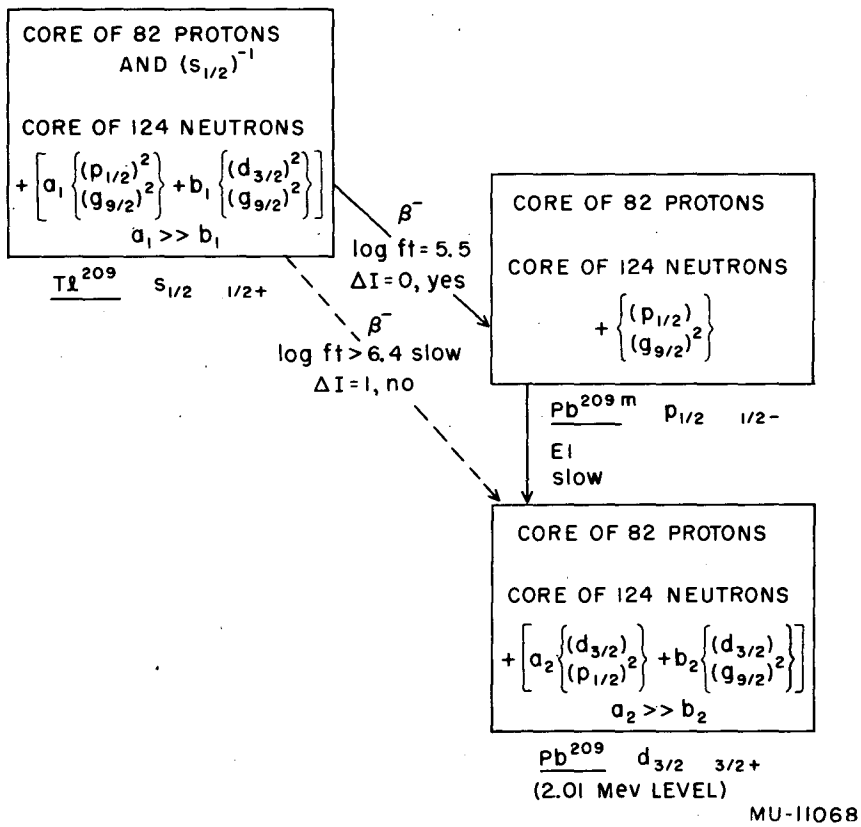

Fig. I-18 Schematic Representation of Principal Nucleon Configurations Involved in Gamma and Beta Transitions in the Decay of Tl^{209} and Pb^{209m}

and parity assignments this beta decay would be first forbidden because of parity change (Fig. 9). De-Shalit and Goldhaber,[51] and also King and Peaslee,[52] have discussed several similar cases in this region. The log ft value of 5.5 fits within King and Peaslee's[52] group of "favored" first forbidden beta transitions ($\Delta j = \Delta I = 0$, not $0 \rightarrow 0$, with a parity change). With our proposed principal configurations the beta transition involves transformation of a $p_{1/2}$ neutron to an $s_{1/2}$ proton, entirely analogous to the beta decay of Tl^{207} and Hg^{205}, both "favored" first forbidden transitions with log ft values of 5.2 and 5.5 respectively.[51, 52]

For the decay scheme and level assignments of Fig. 9 ordinary beta selection rules would give an allowed transition (1/2+ → 3/2+) to the 2.01 -Mev level. Experimentally we can say from comparison of intensities of 450-kev and 120-kev gamma radiation that a direct beta transition to the 3/2+ level must be less than 10 percent as intense as the main beta group, hence its log ft > 6.4. This slowness may be simply explained since the transition is ℓ-forbidden ($\Delta\ell = 2$) and has unfavorable parentage overlap.

b. 1-states. The low-lying 1- states found in even-even nuclei of the radium-thorium region are of considerable interest in that analogous levels do not seem to be found either above or below this region.

The upper limit of 1.2 mμsec was set for the half lives of these levels in Ra^{222} and Th^{226}. According to the Weisskopf formula[2, 3] the transition probability of E1 radiation varies as the third power of the energy. After taking out this Weisskopf energy dependence we find that these transitions could be as hindered as the 59.7-kev E1 transition following Am^{241} alpha decay.[17] However, they are not hindered to any greater extent.

The existence of these 1- levels has not been adequately explained theoretically.

2. Magnetic Dipole Transitions

The only magnetic dipole transitions found to be delayed were those following the alpha decay of Cm^{243}. Hollander et al.[38] have

worked out the level scheme shown in Fig. 19, with the metastable state the 285.6-kev level. The M1 transitions emanating from this level seem to be about 10^4 times slower than the lifetimes predicted by the Weisskopf formula.[2, 3]

The ordinary selection rules ($\Delta I = 0, 1$; no parity change) for M1 transitions are not violated. Therefore, we turn to the unified model[6] of the nucleus for an explanation of this delay. This model describes the features of rotational states in strongly deformed nuclei and also implies definite rules governing the relative reduced transition probabilities (essentially transition probabilities with the energy dependence removed) of gamma transitions within a rotational band, or those from a given nuclear state, to the various members of a rotational band. These rules are presented by Alaga, Alder, Bohr, and Mottelson.[53] In addition to the usual total angular momentum (I) and parity (π) quantum numbers, each state is characterized by the projection value of I on the axis of nuclear symmetry. This new quantum number is called K and is equal to or less than I since it is a projection. The extent to which K is a "good" quantum number will depend, in each instance, upon the degree of validity of the approximations made in the theoretical deviation--for example, the assumption that the rotational motion can be treated independently of the intrinsic motion. These approximations are expected to be most nearly valid in this region of large nuclear deformation. A new selection rule results for gamma radiation, namely $L \geq \Delta K$.

The intensity rules as given by Alaga et al.[53] for the reduced transition probability (denoted by B) ratios for the emission of a given multipole radiation from state i to different members, f and f', of a rotational band are

$$\frac{B(L, I_i \rightarrow I_f)}{B(L, I_i \rightarrow I_{f'})} = \frac{\langle I_i L K_i (K_f - K_i) \mid I_i L I_f K_f \rangle^2}{\langle I_i L K_i (K_f - K_i) \mid I_i L I_{f'} K_f \rangle^2} \qquad (3)^*$$

where $\langle I_i L K_i (K_f - K_i) \mid I_i L I_f K_f \rangle$ is the vector addition coefficient (or Clebsch-Gordan coefficient; the notation used here is the same as that used by Condon and Shortley[54]) for the addition of the angular momenta I_i and L to form the resultant I_f. The K selection rule noted above is

*There are exceptions to this formula but for all cases we shall consider this equation is applicable.

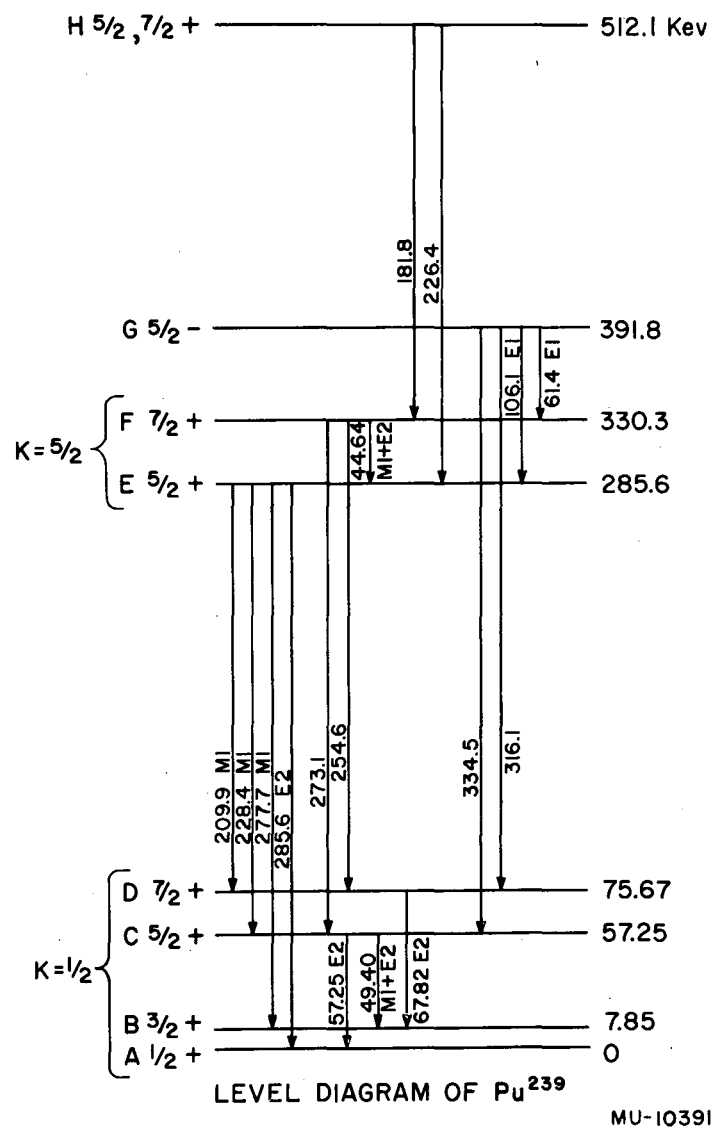

Fig. I-19 Nuclear Levels of Pu^{239}

a direct consequence of Eq. (3), as these Clebsch-Gordan coefficients vanish when $\Delta K > L$. These coefficients have been tabulated by Simon.[55]

The 285.6-kev level has a K quantum number of 5/2, while the ground-state rotational band has K = 1/2. Therefore, the M1 transitions from this 285.6-kev level to the ground-state rotational band involve a ΔK of 2; thus they violate the K selection rule ($L \geq \Delta K$). If this K selection rule were completely rigorous only E2 radiation would be observed. But as Alaga et al.[53] point out, small deviations from the rotational wave functions may serve to relax the K selection rule, which then acts to retard rather than completely eliminate the forbidden multipole radiation.

Hollander et al.[38] have observed that the experimental relative reduced transition probabilities agree with those calculated from the above formula, provided one uses a K_i of 3/2. This indicates that the 285.6-kev level has a component with K = 3/2, and that the M1 transitions proceed only through the K impurity in the initial state.

From the upper limit of E2 mixing set by Hollander et al.[38] in these M1 transitions and the half life of the 285.6-kev level, it can be shown that the E2 gamma transitions from this level are slower by at least a factor of two than what the Weisskopf formula[2,3] predicts.

3. Electric Quadrupole Transitions

The study of E2 transition probabilities in the region of the strongly deformed nuclei is of much interest, as the Bohr-Mottelson theory[6] predicts that these transitions will be greatly enhanced. Most of the E2 transitions investigated in these regions have proved to have half lives much shorter than predicted by the Weisskopf formula.[2-6]

E2 radioactive transitions between members of a rotational band are enhanced through the large electric quadrupole moment of the deformed nucleus. Within the framework of the unified model a measure of the nuclear deformation and of the electric quadrupole moment is provided by the E2 radioactive transition probabilities between rotational states.[6]

Let us first consider the 111.2-kev E2 transition from the 2+ level to the 0+ ground state of W^{184}. The half life of the 2+ level is 9×10^{-10} sec. Thus this E2 transition is about 80 times as fast as

predicted by the Weisskopf formula.[2,3] Therefore the mean life of the E2 gamma ray is 3.9 mμsec. The quadrupole moment of the nucleus is related to the mean life of the E2 transition by Eqns. VII.1 and VII.17 of Bohr and Mottelson.[6] Thus the intrinsic electric quadrupole moment of W^{184} calculated from the mean lifetime of the 2+ state is 7.9 barns (10^{-24} cm.^{2}). This is to be compared with the spectroscopic value[6] of 8 barns obtained for the electric quadrupole moment of Re^{185}, and with the value of 7 barns obtained from the coulomb excitation[6] of W^{184}. From the upper limit set for the half-life of the 72.1-kev E2 transition of Th^{226} we can calculate a lower limit of 4.8 barns for the intrinsic electric quadrupole moment of Th^{226}. Recent coulomb excitation work has shown that the electric quadrupole moments of Th^{232} and U^{238} are about 8 barns.[6,56]

It is interesting to note the correlation of E2 transition lifetimes in even-even nuclides with neutron number. Sunyar[5] has shown that the gamma transition probabilities vary in a smooth fashion with neutron number in the region between the two closed shells of 82 and 126 neutrons. The reduced transition probabilities reach their maximum value about neutron number 100 and decrease as we approach either closed shell. Near the closed shell of 126 neutrons the transition probabilities decrease to the Weisskopf formula prediction[2,3] or even smaller values. All of this is consistent with the unified model,[6] which predicts the enhanced E2 transitions in the region of prolate deformed nuclei. Sunyar's correlation[5] very nicely defines the limits of this region. Beyond the closed shell of 126 neutrons there is another region of strongly deformed nuclei, but there are not enough data available on reduced E2 transition probabilities to define the region as has been done for the rare earth region.

4. Levels of W^{184} Populated by Decay of Re^{184}

In the region where the unified model is applicable, low-lying levels are expected in even-even nuclei with spins 0+, 2+, 4+... These levels lie at energies proportional to I(I+1).[6] It has been noted in a previous section that the energy of the 4+ level in W^{184} was somewhat lower than one calculates from the simple I(I+1) relationship. Sunyar's plot[5] shows that at 110 neutrons we are no longer in the region of

strongest deformation and the Bohr-Mottelson picture[6] should not be expected to hold too well.

If the decay scheme proposed for Re^{184} in Fig. 16 is correct, the 890-kev level must have a spin of two and it must depopulate by quadrupole radiation (from consideration of gamma-radiation lifetimes and conservation of angular momentum) to the three members of the ground-state rotational band. Previous work[40] has shown the existence of a level of W^{182} at 1222 kev which has I and K both equal to 2 with even parity. By analogy we might expect the 890-kev level of W^{184} to have the same quantum numbers.

As accheck on this hypothesis we have the intensity rule of Alaga et al.[53] previously discussed. Table II compares the theoretical reduced photon intensities from a (22+) level to the three members of a rotational band with the experimental values observed in Re^{184} decay. This agreement with the theoretical intensities is the main basis for the I, K, and π quantum numbers shown in Fig. 16. It is interesting to note that this (22+) level seems to be decreasing in energy with increasing mass number. In W^{182} it is at 1222 kev, in W^{184} at 890 kev, and in Os^{186} at 764 kev.[57, 58]

Table II

Experimental and theoretical relative reduced transition probabilities from the 890-kev level of W^{184}

Final State I_f	Experimental $\frac{B(890 \rightarrow I_f)}{B(890 \rightarrow 0)}$	Theoretical ($K_i = 2$; $K_f = 0$)
2+ (111.2 kev)	1.42 ± .14	1.43
4+ (350 kev)	~ .12	0.071

II. APPLICATIONS OF NILSSON'S WAVE FUNCTIONS FOR DEFORMED NUCLEI

A. Introduction

The spherical nuclear shell model[59] has been highly successful in accounting for various regularities in nuclear properties. In this model the nucleons are considered as moving independently in an averaged potential. By choosing a potential containing strong spin-orbit coupling one obtains a progression of single-particle states that explains experimental observations associated with the so-called magic numbers of closed shells.

The potential employed for the shell model is usually assumed to be isotropic. However, it has been found experimentally that nuclei with proton and neutron numbers considerably different from the magic numbers have large deformations. The experimental evidence for this deformation consists of the large quadrupole moments exhibited by many nuclei.[6] This deformation of the nuclear field has an important effect on the motion of individual nucleons.

The introduction of a nonspherical binding field implies that the nuclear shape and orientation must be considered dynamical variables. These variables are associated with collective types of nuclear motion which accompany variations in the binding field. The interplay between these collective and individual-particle modes of motion forms the basis of the unified nuclear model.[6]

The nuclear properties resulting from this interplay are found to depend essentially on the magnitude of deformation.[60] In the region of closed shells the equilibrium shape of the nucleus is spherical and the spherical shell model is applicable to obtain the individual-particle spectrum. The addition of a few more nucleons leads to a nuclear deformation. In this region a very complicated structure of nuclear states may arise owing to the coupling between collective and individual-particle modes of motion.

If the addition of a few more nucleons increases the nuclear deformation to make the nuclei strongly deformed then the situation simplifies.[6, 60] In this case it is possible to separate approximately

between intrinsic nucleonic motion and the collective rotational and vibrational motions, which leave the intrinsic structure unaffected. The separation of the nuclear motion into collective and intrinsic modes corresponds to the assumption of a wave function of the product type as the solution to the nuclear wave equation,[60]

$$\psi = \chi \cdot \phi_{vib} \cdot D_{rot}.$$

Here χ represents the intrinsic motion of the nucleons, which can be expressed in terms of the independent motion of the individual particles in the deformed field. The second factor, ϕ_{vib}, describes the vibrations of the nucleus around its equilibrium shape, while D_{rot} represents the collective rotational motion of the system as a whole.

Deformed nuclei are expected to prefer geometric configurations with cylindrical symmetry, hence only particle states in a spheroidal-type deformation are considered. In this case of axial symmetry, the intrinsic motion is characterized by the quantum numbers Ω_p, the component of angular momentum of each nucleon along the nuclear axis.[6] The total Ω is then given by $\Sigma\Omega_p$. States are doubly degenerate (corresponding to $\pm\,\Omega_p$), and the total χ is therefore the antisymmetrized product of individual-particle wave functions χ_{Ω_p}.

The rotational motion is characterized by the quantum numbers I, M, and K, i.e., the total angular momentum (spin), its projection on the space-fixed axis (z'') and its projection on the intrinsic nuclear axis (z'; this axis will hereafter be called the nuclear symmetry axis), respectively.[6] (See Fig. 1)

We shall always assume that we are in the vibrational ground state; therefore, we shall not be concerned with the vibrational quantum numbers.

Nilsson[60] has considered the problem of binding states of nucleons in a spheroidal deformed potential. For the sake of simplicity Nilsson first chose a three-dimensional harmonic oscillator potential. The usual spin-orbit term was also included. The final term in the Hamiltonian is a term in $\vec{\ell}^{\,2}$ which gives a correction to the oscillator potential to make it correspond more closely to a square-well potential. The relative contributions of the spin-orbit and $\vec{\ell}^{\,2}$ terms are determined in the spherical case by requiring that the Hamiltonian yield the

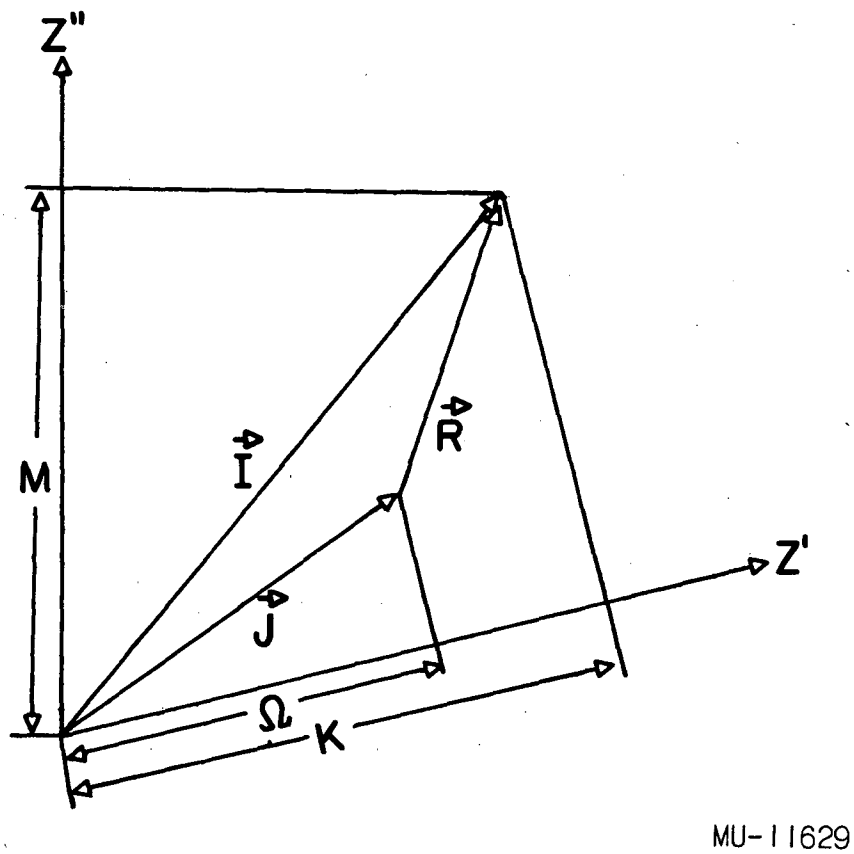

Fig. II-1 Angular Momentum Diagram

empirical known sequence of single-particle levels considered in the spherical shell model.[59]

For the purposes of the calculations for spheroidal deformation Nilsson[60] introduces two parameters of deformation, η and δ (where η is a function of δ), to make the harmonic oscillator potential anisotropic. The parameter δ is related to the quantity β used by Bohr and Mottelson[6] to first order as

$$\delta \approx 0.95\,\beta\,.$$

The basic vectors $|N\ell\Lambda\Sigma\rangle$ are used to describe the states corresponding to a given Ω. Here N represents the total number of oscillator quanta, ℓ is the total orbital angular momentum, and Λ and Σ represent the projections of ℓ and the intrinsic spin s on the symmetry axis. In this representation $\Omega = \Lambda + \Sigma$. This is a convenient representation, since these basic vectors are orthonormal. As an approximation in the calculations Nilsson[60] considered only nonvanishing matrix elements of the Hamiltonian between basic vectors having the same N and Ω.

Nilsson[60] has tabulated the eigenfunctions of the states for various values of the deformation parameter η in terms of the above basic vectors. Nilsson has also tabulated the energy eigenvalues as functions of the deformation parameters. From these eigenvalues he has plotted an energy-level diagram of the various states as a function of deformation. This plot is convenient to use for correlating Nilsson's states with actual nuclear states.

It is the aim of this section to consider various applications of Nilsson's wave functions[60] to see how useful they are for explaining experimental data.

As the spectrum of particle states--as well as the properties of a particular state--depends essentially on the deformation parameter we must have an estimate of this quantity before we can consider detailed properties of intrinsic structure. An independent estimate of the deformation parameter δ can be obtained from the empirically determined quadrupole moment. Nilsson[60] has given the following approximate relationship

$$Qo \approx 0.8\ Z\ R^2\ \delta\ (1 + 2/3\ \delta),$$

where Qo is the intrinsic quadrupole moment, Z is the atomic number of the nuclide, and R is the radius of charge of the nucleus ($\approx 1.2 \times 10^{-13}\ A^{1/3}$ cm).

The region of strongly deformed nuclei in between the closed shells of 82 and 126 neutrons has been considered in detail by Mottelson and Nilsson.[61] In this region the largest deformation found corresponds to a deformation parameter δ of about +0.3. In the actinide series the few quadrupole moments measured[6, 56, 62] (U^{238} and Th^{232}) indicate that the deformation parameter δ has a value of about +0.21. However, there are not sufficient data available to know if this value will hold throughout the actinide region.

For the purposes of these applications it will be assumed that the strongly deformed nuclei have a prolate spheroidal deformation.

Manning et al.[62] have measured the quadrupole moments of Am^{241} and Am^{243} and have verified the prolate deformation of these two nuclei.

Figure 2 is a reproduction of part of Nilsson's energy-level diagram.[60] Only that region of the diagram which is of interest is shown. In addition, several other states whose energy eigenvalues were calculated but not plotted by Nilsson are also shown. The energy eigenvalues of the various nucleon states emanating from the $j_{15/2}$ orbital have not been calculated, and their positions in Fig. 2 are only estimated.

B. Applications

1. Decoupling Parameters

We shall consider odd-mass nuclei that are well removed from closed shells. For these nuclei, one may separate with fair accuracy between collective rotational motion and the intrinsic motion of the nucleus.[6] With each intrinsic state of the system there is associated a rotational band having members of spin $I = I_o = K$, $K+1$, $K+2$.... These states have rotational energies[6] proportional to $[I(I+1) - I_o(I_o+1)]$, provided $I_o = \Omega = K > 1/2$.

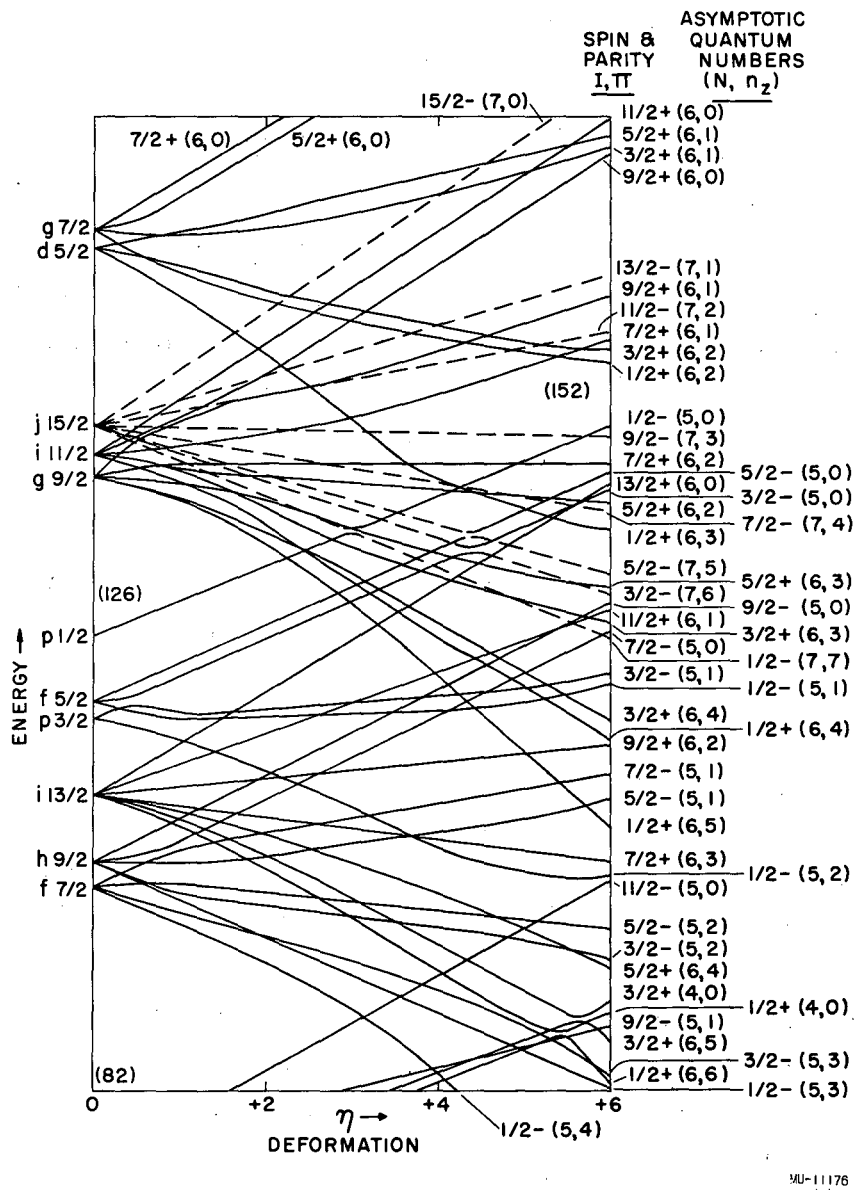

Fig. II-2 Nilsson's Energy-Level Diagram

Intrinsic states with $K = 1/2$ are especially interesting since, in this case, there may occur a partial decoupling of the intrinsic spin of the last odd nucleon from the rotational motion.[6] This decoupling, which depends on the intrinsic structure, manifests itself in such properties as the rotational-energy spectrum and the magnetic moment. The decoupling parameter $\underline{a}$ appears in the following expression[60] for the energy of the members of a rotational band with $K = 1/2$:

$$E_{rot} = A\,[\,I\,(I+1) + \underline{a}\,(-)^{I+1/2}(I+1/2)] \qquad (4)$$

where A has a constant value for a particular rotational band. It is interesting to correlate the experimental values of $\underline{a}$ with those calculated from Nilsson's wave functions.[60] The appropriate formula used in this calculation is Eq. (19) of Nilsson.[60] Mottelson and Nilsson[63] have already considered the decoupling parameter of Tm^{169} and have shown that their calculated value gives excellent agreement with the experimentally observed quantity.

The recent studies[38-40] of the nuclear properties of Pu^{239} and W^{183} by means of high-resolution electron and gamma spectroscopy have yielded a considerable amount of data on the rotational spectra of these two nuclides. The ground-state spin of both nuclei[64, 65] has the value $I_o = 1/2$. Thus, it is possible to obtain an accurate experimental decoupling parameter in each case.

We shall first discuss Pu^{239}. Hollander et al.[38] have obtained an experimental value of $\underline{a} = -0.58$. The first test of Nilsson's wave functions[60] is whether there is available an orbit at N = 145 neutrons. For this purpose we shall assume a deformation parameter of $\delta = +0.2$ (corresponding to $\eta = +4$). From an examination of Fig. 2 we see that there are two orbits which should be filled at about N = 145. In Nilsson's notation[60] these are states A and B.

The values of $\underline{a}$ calculated for states A and B as a function of deformation are shown in Fig. 3. Clearly, state A does not agree with the experimental value, while state B does yield a decoupling parameter in rough agreement with the experimental data at a deformation parameter of $\eta = +4$. Hence Nilsson's orbit B[60] will be designated as the state corresponding to the ground level of Pu^{239}. As state B has even parity, it is predicted that the ground state of Pu^{239} will also

have even parity.

It is interesting to note that the favored alpha decay of Pu^{239} populates[66] three excited levels of U^{235} with a relatively unhindered alpha population to the lowest of the three levels. If we assume that these three states constitute the members of a rotational band with $I_0 = 1/2$, then we can calculate the experimental decoupling parameter $\underline{a} \approx -0.25$ from the data of Freedman et al.[67] It is reasonable to assume that the level which is populated by relatively unhindered alpha decay has the same intrinsic nucleonic wave function as the ground state of the parent nuclide. Hence Nilsson's orbit B[60] is designated as the level corresponding to the excited levels of U^{235}. Fig. 3 shows that the calculated value of $|\underline{a}|$ for orbit B decreases with a decrease of the deformation parameter.

Thus, we would expect U^{235} to be somewhat less deformed than Pu^{239}. Unfortunately, the quadrupole moments of the two nuclides have not been measured; therefore a comparison with experimental data is not possible at this time.

Mottelson and Nilsson[61] have designated Nilsson's State 71 as the orbit corresponding to the ground state of W^{183}. A deformation parameter of $\eta = +4$ is estimated[61] for this nucleus. Figure 4 shows the calculated value of the decoupling parameter as a function of deformation compared with the experimental value of $\underline{a} = +0.19$ calculated from the data obtained by Murray et al.[40] Thus, there is rough agreement between the calculated and experimental values at the expected deformation of the W^{183} nucleus.

2. Magnetic Moments

The comparison of calculated and experimental magnetic moments gives us another critical test of Nilsson's wave functions[60] in the heavy region. Unfortunately there are not many accurate measurements of magnetic moments in this region available at present. As more magnetic-moment data become available, more definite conclusions can be reached.

Nilsson's Formulae (24)-(26)[60] are the appropriate equations used for the calculations of magnetic moments of deformed nuclei. We shall reproduce two of these formulae here. For the case

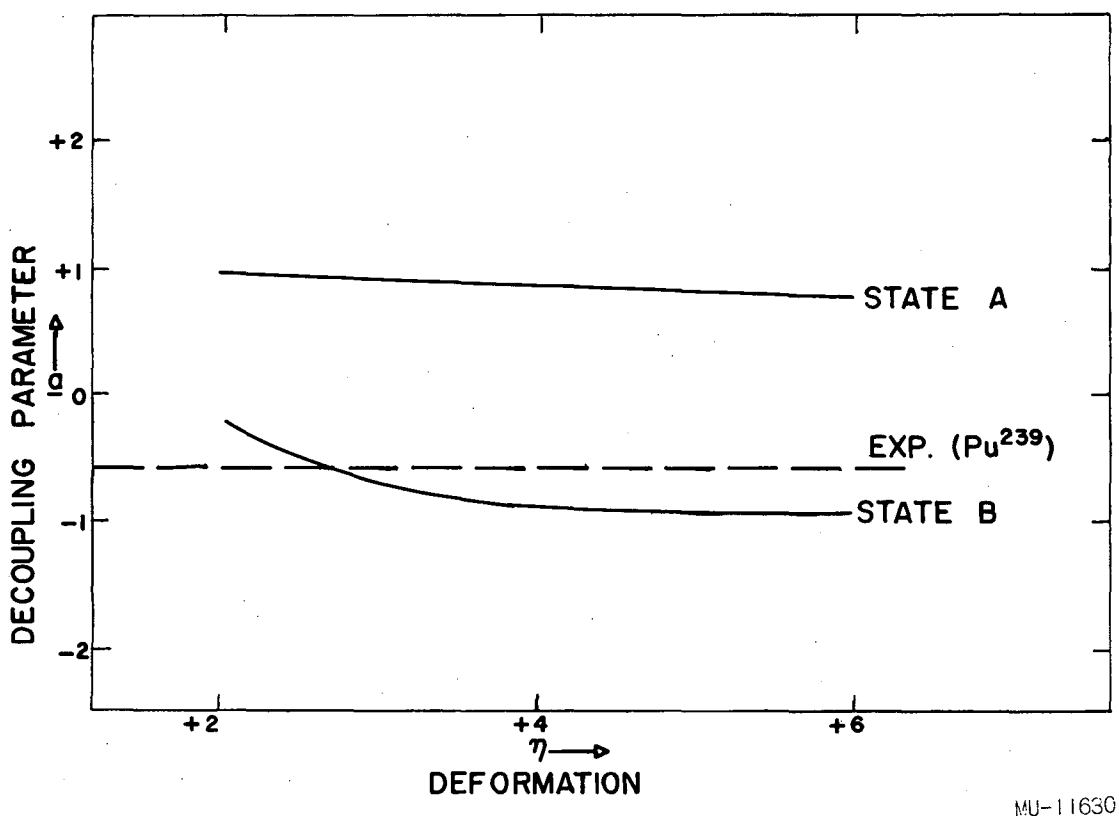

Fig. II-3 Calculated and Experimental Decoupling Parameters for Pu^{239}

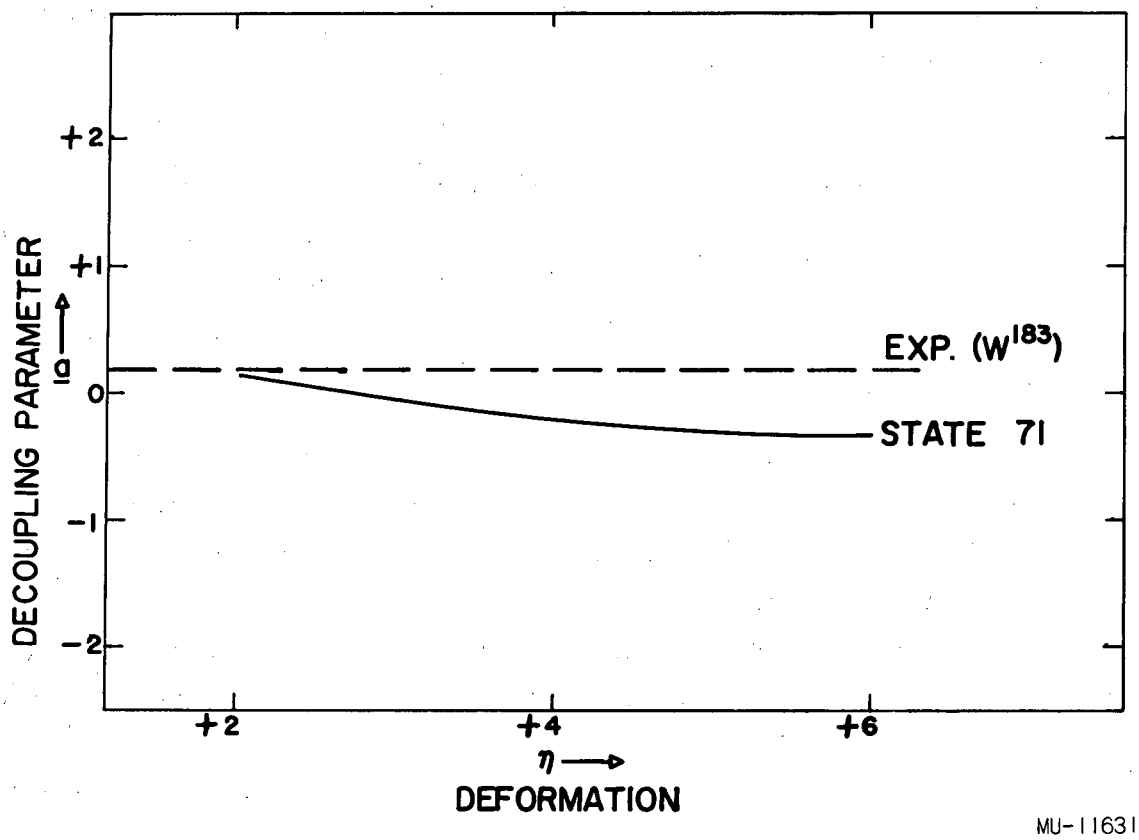

Fig. II-4 Calculated and Experimental Decoupling Parameters for W^{183}

$I = \Omega = K (\neq 1/2)$, the magnetic moment is given by

$$\mu = \frac{I}{I+1} \left[(g_s - g_\ell) 1/2 \sum_\ell (a^2_{\ell \Lambda = \Omega - 1/2} - a^2_{\ell \Lambda = \Omega + 1/2}) + g_\ell I + g_R \right], \quad (5)$$

where g_s and g_ℓ are the intrinsic and orbital g-factors. In nuclear units their values are

$$g_s = \begin{bmatrix} 5.585 \\ -3.826 \end{bmatrix} ; \quad g_\ell = \begin{bmatrix} 1 \\ 0 \end{bmatrix} , \quad (6)$$

where the upper values apply for a proton and the lower ones for a neutron. Here g_R is the g-factor for the angular momentum carried by the surface. We shall assume

$$g_R \approx Z/A, \quad (7)$$

where Z is the atomic number of the nuclide and A is its mass. The quantities $a_{\ell, \Lambda = \Omega \pm 1/2}$ refer to the normalized coefficients of the basic vectors employed to characterize Nilsson's states.[60]

For the case $I = \Omega = K = 1/2$ and odd parity, the magnetic moment is expressed by

$$\mu = 1/3 \left[(g_\ell - g_R) \underline{a} - 1/2 \, g_s + g_\ell + g_R \right] . \quad (8)$$

Thus in this particular case there is a relationship between the decoupling parameter $\underline{a}$ and the magnetic moment μ that is independent of the nucleonic wave functions.

The magnetic moment of Pu^{239} has been experimentally measured by Bleaney et al.[68] Their value of the magnetic moment is $|\mu| = 0.4 \pm .2$ nuclear magnetons. Formula (25) of Nilsson[60] was used for the calculation of the magnetic moment of orbit B. Figure 5 shows the calculated value of μ as a function of deformation compared with the experimental value. In this case the agreement is well within the experimental error at a deformation of $\eta = +4$. It should be noted that only the magnitude of the magnetic moment is known experimentally and that the calculated values predict that the magnetic moment of the ground state of Pu^{239} is negative.

The magnetic moment of W^{183} has been accurately measured by Sogo and Jeffries[69] and has been found to have the value of +0.115 nuclear magnetons. Nilsson's[60] orbit 71 has odd parity, therefore we

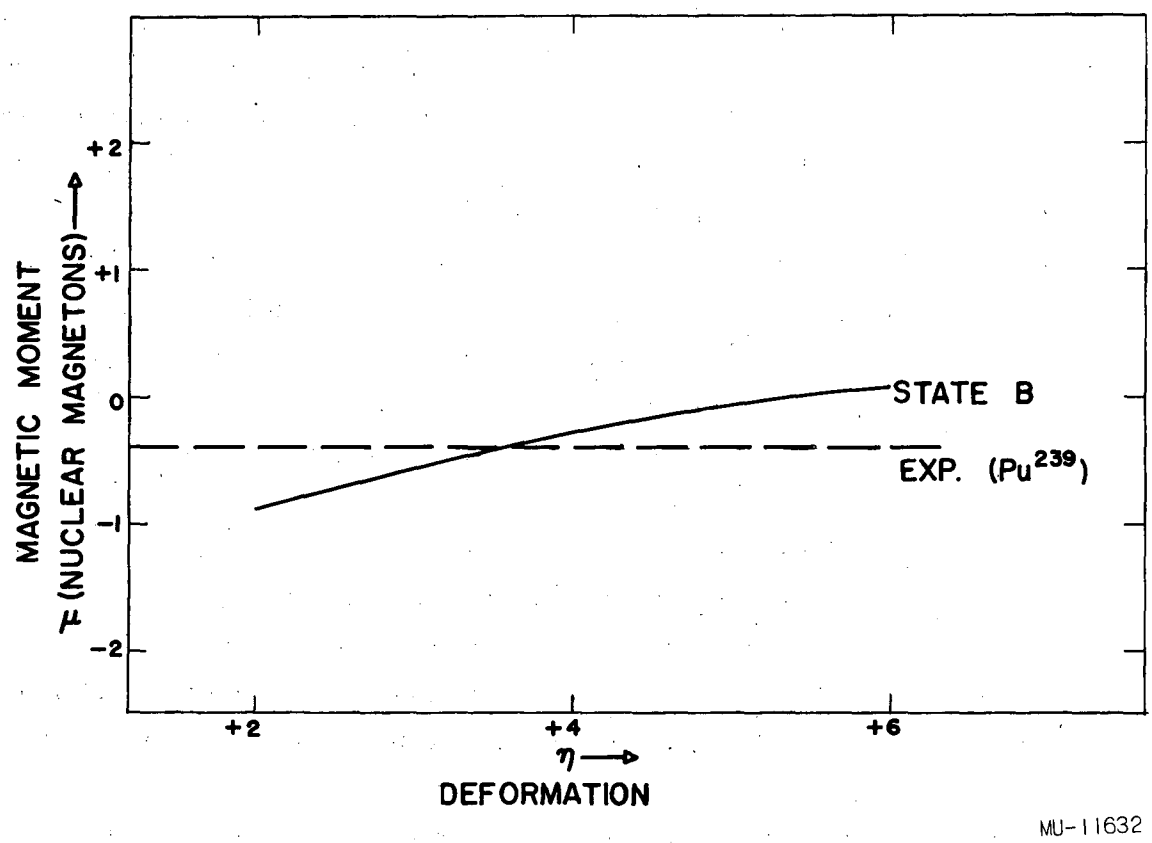

Fig. II-5 Calculated and Experimental Magnetic Moments for Pu^{239}

may use Eq. (8) above for the calculation of the magnetic moment of the ground state of W^{183}. If we use the calculated values of a we find that the calculated magnetic moment ranges from +0.75 to +0.82 nuclear magnetons for values of η varying from +2 to +6. Thus, in this case there is very poor agreement between the experimental and calculated values. Moreover, if one repeats this calculation using the experimental value of a, one still obtains a value for the magnetic moment in complete disagreement with the experimental μ.

The magnetic moment of the ground state of Np^{237} has been measured and found to be 6 ± 2.5 nuclear magnetons by Bleaney et al.[70] The ground-state spin of Np^{237} has been measured as 5/2 by Tomkins.[71] An examination of Fig. 2 reveals that there are two orbitals with $\Omega = 5/2$ which should be filled at about Z = 93. In Nilsson's notation[60] these are states 44 and 55. These two levels differ in parity, which correlates well with the existence of a low-lying level in Np^{237} with parity opposite that of the ground state. We shall refer to this state as Np^{237m}. Np^{237m} has been assigned[72] a spin value of 5/2 mainly on the basis of rotational structure. Alpha-gamma angular correlation work[73] from the decay of Am^{241} is also consistent with the spin of Np^{237m} being 5/2.

Krohn et al.[74] have measured a g-factor of $+0.8 \pm 0.2$ for Np^{237m} by measuring the attenuation of the alpha-gamma angular anisotropy in an applied magnetic field. Therefore, assuming the spin value of Np^{237m} is 5/2, we find that the experimental magnetic moment μ is 2.0 ± 0.5 nuclear magnetons. Figure 6 shows the experimental values of μ for Np^{237} and Np^{237m}.

Figure 6 shows the calculated magnetic moments of states 44 and 55 as a function of deformation. Equation (5) above was used for this calculation.

On the basis of these calculations it seems reasonable to assign Nilsson's[60] orbitals 55 and 44 as the states corresponding to the ground state of Np^{237} and Np^{237m} respectively. Thus according to these designations the ground state of Np^{237} has even parity and Np^{237m} has odd parity.

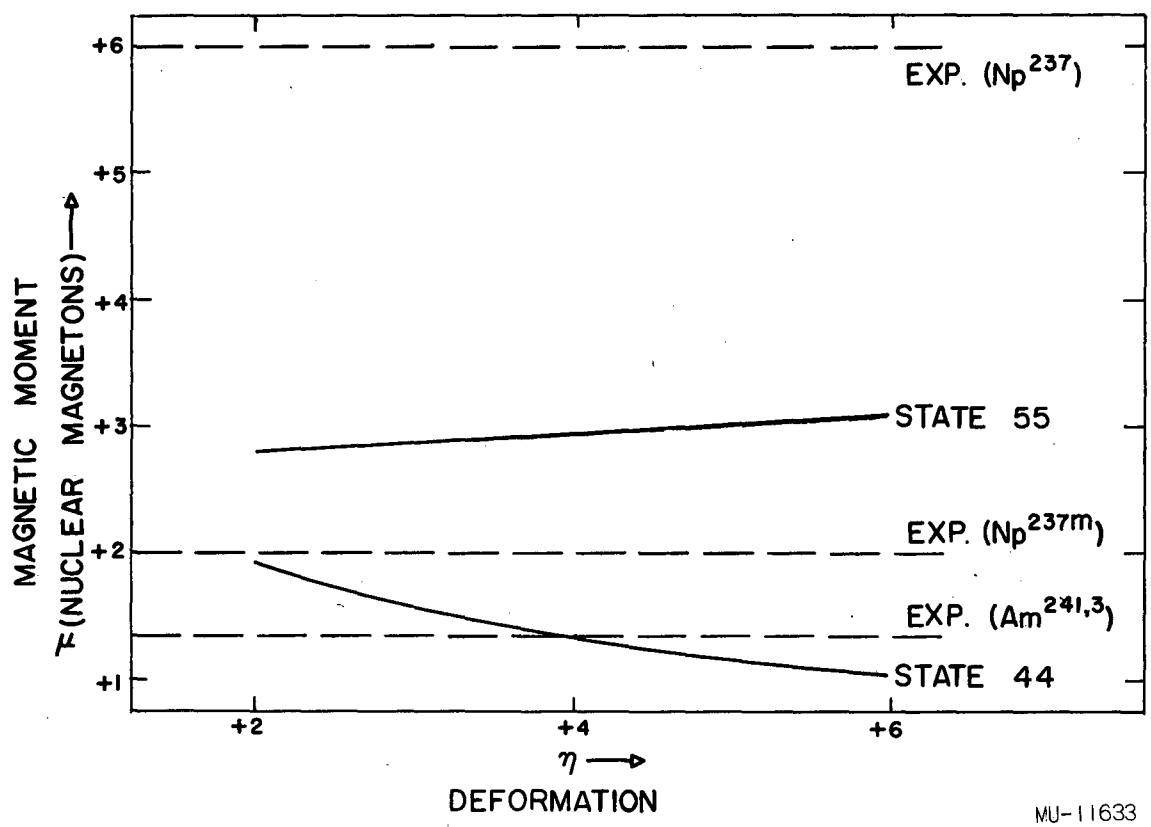

Fig. II-6 Calculated and Experimental Magnetic Moments for $Am^{241,3}$, Np^{237}, and Np^{237m}

Some comments are in order on the discrepancy between the experimental μ of +6 nuclear magnetons and the calculated value of about +3 nuclear magnetons for the ground state of Np^{237}. According to Eq. (5) above, the maximum value of μ occurs when the sum of the normalized coefficients is equal to unity. Thus the maximum value of μ according to Eq. (5) is +3.7 nuclear magnetons for a state with $I = \Omega = K = 5/2$. The large limits of error placed on the experimental value just barely include this maximum value. Hence a more precise determination of the magnetic moment is in order.

The above calculations assume states with a pure K quantum number. Rasmussen[75] has considered the problem of small K admixtures, and has shown that small impurities in the states can have some effect on the magnetic moments. The effect does not seem large enough, however, to bring the calculated magnetic moment up to the experimental +6 nuclear magnetons.

Manning et al.[62] and Conway and McLaughlin[76] have measured the magnetic moments of Am^{241} and Am^{243}. Manning et al. obtained a value of $\mu = +1.4$ nuclear magnetons, and Conway and McLaughlin obtained a value of $\mu = +1.3$ nuclear magnetons for both nuclides. Both nuclei have a ground-state spin of 5/2;[77, 78] therefore we should expect Nilsson's orbit 44 or 55 to correspond to the ground states of Am^{241} and Am^{243}.[60] This experimental value of the magnetic moment is also shown in Fig. 6. Clearly the calculated value of orbital 44 agrees more closely with the experimental value. Thus, Nilsson's[60] orbit 44 is designated as the level corresponding to the ground states of Am^{241} and Am^{243}.

There is available one more piece of data which illustrates the self-consistency of the above designations. In alpha decay it is expected that unhindered alpha population proceeds to that level having the same nucleonic wave functions as the initial state. Thus we would expect unhindered alpha decay of Am^{241} to Np^{237m}. Experimentally, this is just what is observed.[79]

3. Electric Dipole Transition Probabilities

The application of Nilsson's orbitals[60] to the study of E1 transitions is of much interest. The mere existence of low-lying E1 transitions in the actinide region is one of the major shortcomings of the spherical nuclear shell model.[59,72] According to this shell model, there is only one level with even parity available between 82 and 126 nucleons. This is the $i_{13/2}$ level. All the other states have odd parity and the $h_{9/2}$ level has the highest j-value of these. E1 transitions require a parity change; therefore, according to the shell model an E1 transition for an odd-Z nucleus in the actinide region must occur between the $i_{13/2}$ and one of the odd-parity orbitals. However, any of these transitions requires a $\Delta I_{min} = \Delta j \leq 2$. Thus, the selection rules for E1 transitions are violated, and the presence of low-energy E1 transitions in the actinide region is inconsistent with the spherical shell model.

In the region of strongly deformed nuclei the projection of the total $\vec{J}$ on the nuclear symmetry axis is a "good" quantum number and is denoted by Ω.[6,60] (See Fig. 1.) In an odd-A nucleus the ground-state spin is equal to the value of Ω for the orbit occupied by the last odd nucleon (with the possible exception when $\Omega = 1/2$). Figure 2 shows Nilsson's energy-level diagram for the heavy region.[60] It should be noted that there are many deviations from the usual shell-model rules as to relation of spin and parity in a given shell. It should also be noted that low-lying E1 transitions no longer violate the ΔI selection rules since there are many close-lying orbitals which differ in parity and have $\Delta I = \Delta\Omega = 0, \pm 1$.

Many E1 transition probabilities in the actinide region have been experimentally determined. We restrict ourselves here to odd-Z nuclei because more data are available for them, and also because Nilsson's wave functions[60] are not extensive enough to consider the odd-neutron cases. The available data for odd-Z nuclei are summarized in Table I. Figure 7 shows a plot of the E1 transition lifetimes as a function of Z. To remove the energy and mass dependence (according to the Weisskopf formula[2,3] the transition probabilities of electric transitions vary directly as E^{2L+1} and $A^{2L/3}$),

the mean lifetimes are multiplied by the factor $E^3A^{2/3}$. Figure 7 also shows the Weisskopf prediction[2, 3] for these E1 transition lifetimes.

It is evident that some of these E1 transitions are of the order of 10^5 times slower than the value calculated from the Weisskopf formula.[2, 3] Moreover, in the cases of the actinium and neptunium isotopes, there seems to be an erratic variation of the E1 transition probabilities. On the other hand, the E1 transition probabilities for the protactinium isotopes exhibit some striking similarities. The 85-kev transition of Pa^{231} and the 87-kev transition of Pa^{233} not only are both delayed, but have just about the same reduced transition probability. The lower-energy E1 transitions of the two protactinium isotopes also show similar behavior.

The notion of K-forbiddenness has succeeded in explaining some other delayed transitions (i.e., see the discussion of M1 transitions of Pu^{239} in Part I of this paper). However, there are at least two nuclides whose energy levels are well known (W^{182} and Np^{237}) and for which definite K and I quantum numbers may be assigned to the energy levels.[53, 80] In these two cases delayed E1 transitions have been observed, but the K quantum-number assignments do not indicate any K-forbiddenness involved.

Thus, detailed calculations of E1 transition probabilities were undertaken, using Nilsson's wave functions,[60] to see if they could explain the erratic behavior of E1 transition lifetimes in the actinide region.

To calculate E1 transition probabilities for specific nuclei we must know the wave functions for the initial and final states; therefore, we must also know the Nilsson's orbits[60] corresponding to the nuclear states. In general we do not have this information. On the basis of magnetic-moment calculations described previously, Nilsson's[60] orbital 55 was designated as the level corresponding to the ground state of Np^{237}, while Nilsson's orbital 44 seems to have the same properties as Np^{237m} and Am^{241}. Thus, we can use the wave functions of these two states to calculate the E1 transition probability of the 59.6-kev gamma ray of Np^{237m}. We cannot make specific

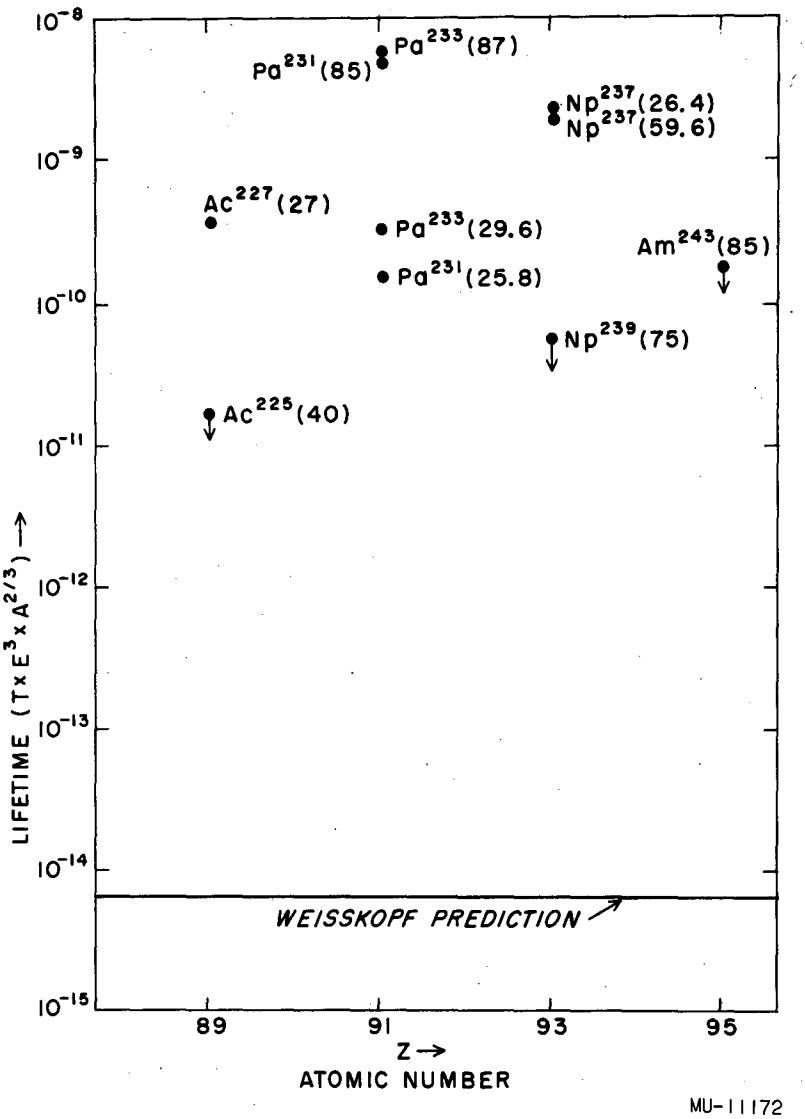

Fig. II-7 Experimental El Transition Lifetimes in the Actinide Region

Table I

Data for E1 transition lifetimes for odd-Z nuclei in the actinide region

Daughter Nucleus	Energy of gamma (Mev)	Partial half-life of photon (seconds)	Reference
$^{148}_{95}Am^{243}$	.085	$<5 \times 10^{-9}$	81, 82
$^{146}_{93}Np^{239}$	.075	$<2 \times 10^{-9}$	24 - 26
$^{144}_{93}Np^{237}$	.0596	1.6×10^{-7}	17
$^{144}_{93}Np^{237}$	.0264	$2.2_5 \times 10^{-6}$	17
$^{142}_{91}Pa^{233}$	.087	1.5×10^{-7}	18, 19
$^{142}_{91}Pa^{233}$	.0296	2.2×10^{-7}	18, 19
$^{140}_{91}Pa^{231}$	.085	1.4×10^{-7}	18
$^{140}_{91}Pa^{231}$	.0258	1.5×10^{-7}	18
$^{138}_{89}Ac^{227}$	.027	3.6×10^{-7}	20
$^{136}_{89}Ac^{225}$	.040	$<4.2 \times 10^{-9}$	18

comparisons for the other E1 transitions in the actinide region; however, a number of E1 transition probabilities were calculated for various combinations of Nilsson's orbitals which probably correspond to the nucleonic states of actinium, protactinium, neptunium, and americium. The interest here was to see the general trend of the calculated values.

The transition probability for a gamma transition of frequency ω and multipolarity L is given by

$$T(L) = \frac{8\pi(L+1)}{L[(2L+1)!!]^2 \hbar} \left(\frac{\omega}{c}\right)^{2L+1} (B(L)), \qquad (9)$$

where $(2L+1)!! = (2L+1)(2L-1)\ldots\ldots 3\cdot 1$, and B(L) is the reduced transition probability.

We shall consider two cases. First we shall assume that the radial wave function is constant within the nuclear volume and vanishes outside. Then, for a single proton transition with $K + K' \geq L$, it can be shown that the reduced transition probability for an E1 transition is given by

$$B(E1,\ I \rightarrow I') = e^2(1 - Z/A)^2 \left(\frac{3\ R_o}{4}\right)^2 \frac{3}{4\pi} \left|\langle I1\,K(K'-K) | I1\ I'\,K'\rangle\right|^2 \qquad (10)$$

$$\left[\sum_{\ell'\ell} \sqrt{\frac{2\ell+1}{2\ell+1}} \langle \ell\,100 \mid \ell 1 \ell' 0\rangle \sum_{\substack{\Lambda' \\ \Sigma'}} \sum_{\substack{\Lambda \\ \Sigma}} \delta_{\Sigma'\Sigma}\ a'_{\ell'\Lambda}\ a_{\ell\Lambda} \langle \ell 1 \Lambda (K'-K) \mid \ell 1 \ell' \Lambda'\rangle\right]^2$$

where the following notation is used:

e is the charge on the proton,

Z is the atomic number of the nuclide,

A is the mass of the nucleus,

R_o is the nuclear radius ($= 1.44 \times 10^{-13} A^{1/3}$ cm).

$\langle j_1 j_2\ m\ m \mid j_1 j_2\ m\rangle$ is the Clebsch-Gordan coefficient (in the notation of Condon and Shortley[54]) for the addition of the angular momentum vectors $\vec{j}_1$ and $\vec{j}_2$ to form a resultant $\vec{j}$ with component m,

Σ is the projection of the intrinsic spin on the nuclear symmetry axis ($\Sigma = \pm 1/2$).

$\delta_{\Sigma\Sigma'}$ is the Kronecker delta symbol $\begin{bmatrix} = 0, & \text{if } \Sigma' \neq \Sigma \\ 1, & \text{if } \Sigma' = \Sigma \end{bmatrix}$

$a_{\ell\Lambda}$ refers to the normalized coefficients of the basic vectors employed to characterize Nilsson's[60] orbits.

The primed symbols refer to the final state and the unprimed symbols refer to the initial state.

Equation (10) was used for calculations at deformations of $\eta = +2$, $+4$, and $+6$. Figure 8 shows the results of these calculations for the case of deformations of $\eta = +4$ and $+6$. The data of Fig. 7 have also been reproduced on this graph for comparison purposes. The spread of the calculated values indicates how much the transition probability varies as the deformation parameter η changes from +4 to +6.

From this figure we observe that the calculated values indicate that there is a general trend towards slowing down E1 transitions. The center of gravity of the calculated values seems to be fairly close to the center of gravity of the experimental data. The specific calculation for the E1 transition of Np^{237} also seems to be in fair agreement with the experimental value.

It is also possible to carry out these calculations without making the radial wave function assumption used above. In this case the appropriate formulae are Eqs. (35), (41), and (42) of Nilsson's.[60] Figure 9 shows the results of these calculations for the same orbitals at the same deformations. It should be noted that in this case the E1 transition probability varies as $A^{1/3}$. Hence the experimental mean lifetimes are multiplied by the factor $E^3A^{1/3}$ to remove the energy and mass dependence of the transition probabilities. The general trend of Fig. 9 seems to be much the same as Fig. 8. In specific cases, however, there seem to be considerable changes. For example, the calculated E1 transition probabilities between orbitals 55 and 44 no longer agree with the experimental value for the 59.6-kev E1 transition of Np^{237m}.

Chase and Wilets[83] have calculated E1 transition probabilities, using Nilsson's orbits[60] corresponding to nuclear levels of Lu^{175}. They have noted that the calculated transition probabilities yield a value about 10^4 times smaller than the Weisskopf formula[2,3] would estimate. There is a delayed E1 transition[84] emanating from one of the levels of Lu^{177}. Presumably, the same nucleonic levels are involved in the E1 transition in the two nuclei. The experimental

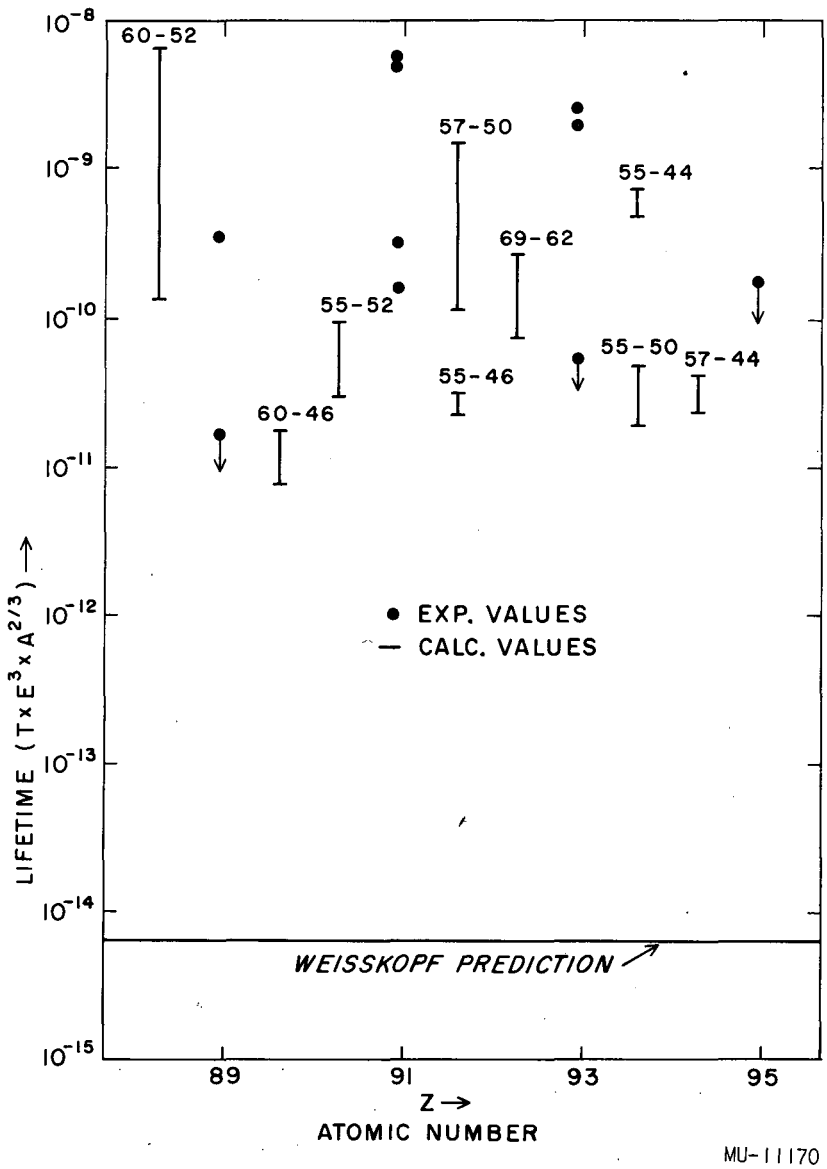

Fig. II-8 Calculated El Transition Lifetimes in the Actinide Region using a Constant Radial Wave Function

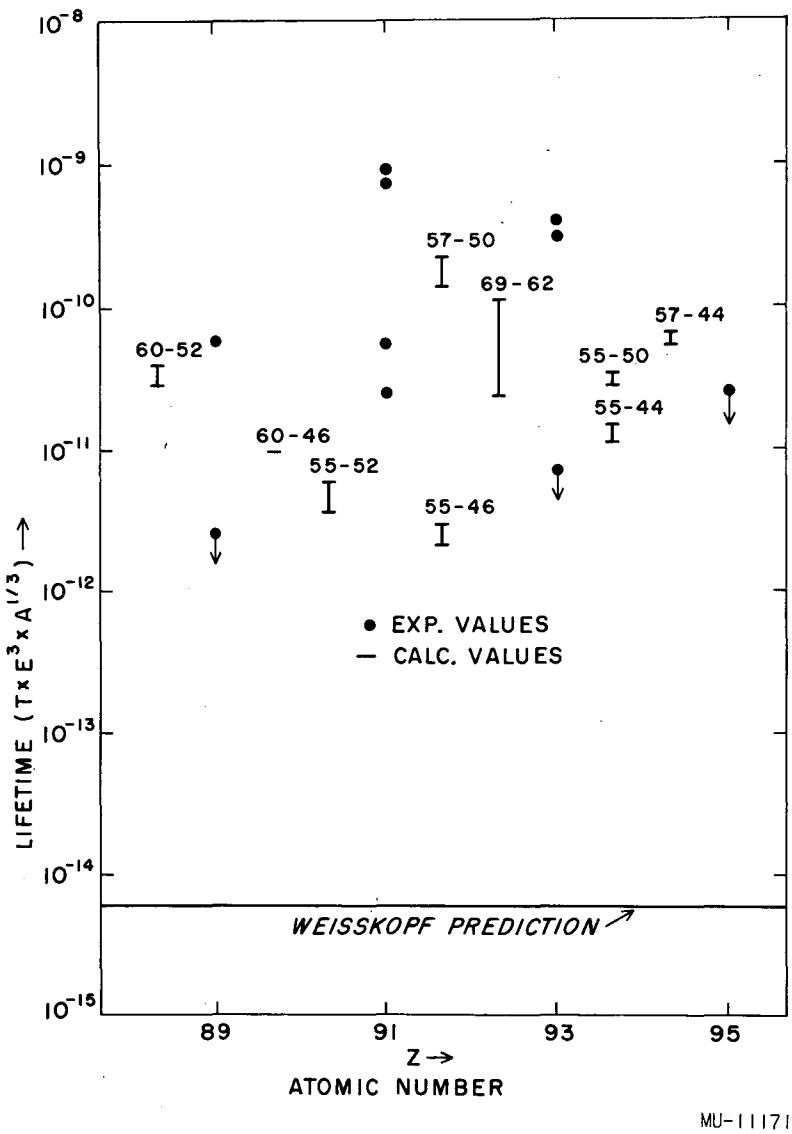

Fig. II-9 Calculated El Transition Lifetimes in the Actinide Region Using a Harmonic Oscillator Radial Wave Function

transition probability of the E1 transition in Lu^{177} is about 10^6 times smaller than the Weisskopf[2, 3] formula prediction. Thus, in this case too, there is only qualitative agreement.

C. Discussion of Results

1. Assignments of Ground-State Spins

Mottelson and Nilsson[61] have already discussed the classification of nucleonic states in the rare-earth region and have noted that there is general agreement between Nilsson's energy-level diagram[60] and the experimental data.

In the actinide region there is also some general agreement between Nilsson's energy-level diagram[60] and the experimentally observed ground-state spins. The one possible exception to this agreement is the ground-state spin of Np^{239}, recently measured and found to have the value $I = 1/2$ by Conway and McLaughlin.[85] Nilsson's[60] Orbit 63 has the spin value $\Omega = 1/2$, but this orbit should be filled at $Z = 97$ instead of at $Z \approx 93$. The correlation of experimental nuclear level spins with possible Nilsson's orbits[60] is summarized in Table II. The deformation parameter was assumed to be +0.2 to +0.3 for all cases considered. In those cases where one of the possible theoretical levels uniquely reproduces the observed properties of the nuclear ground state we list that particular orbit only.

2. Decoupling Parameters and Magnetic Moments

In general, the calculated decoupling parameters and magnetic moments seem to be in qualitative agreement with the experimental values. Thus, Nilsson's wave functions[60] are useful for estimating these nuclear properties when one of Nilsson's orbits[60] may be unambiguously assigned as corresponding to a nuclear level.

In the specific calculation for the magnetic moment of W^{183} a serious discrepancy was noted. At this moment no simple explanation is evident. There is the possibility that the lowest state in the level scheme proposed by Murray et al.[40] is not actually the ground state. A review of Nilsson's energy-level diagram[60] (Fig. 2) does show the presence of another orbital (State 69) with a spin value of 1/2 which should be filled at about $N = 109$. However, the calculated magnetic

Table II

Nuclear-level spins in the actinide region

	Nucleus	Nilsson's Orbits	I, Theoretical	I, Experimental
	$^{148}_{95}Am^{243}$	44	5/2-	5/2
	$^{146}_{95}Am^{241}$	44	5/2-	5/2
	$^{146}_{93}Np^{239}$	55, 44, 52	5/2+, 5/2-, 3/2-	1/2
odd Z	$^{144}_{93}Np^{237m}$	44	5/2-	5/2
	$^{144}_{93}Np^{237}$	55	5/2+	5/2
	$^{140}_{91}Pa^{231}$	52, 57	3/2-, 3/2+	3/2
	$^{138}_{89}Ac^{227}$	57, 52, 60	3/2+, 3/2-, 1/2+	3/2
	$^{147}_{94}Pu^{241}$	many	1/2+, 1/2-, 5/2+ 5/2-, 7/2-	5/2
odd N	$^{145}_{94}Pu^{239}$	B	1/2+	1/2
	$^{143}_{92}U^{235}$	several	1/2+, 7/2+, 5/2+ 5/2-, 5/2-	7/2
	$^{141}_{92}U^{233}$	several	1/2+, 5/2+, 7/2+ 5/2-, 7/2-	5/2

moment (μ calc = -1.2 nuclear magnetons) for this state at $\eta = +4$ is also in disagreement with the experimental value.

McClelland et al.[43] and also Stelson and McGowan[7] have studied the coulomb excitation of natural and separated isotopes of wolfram. Their results are consistent with the idea, but do not prove, that the lowest state in the proposed level scheme is the ground state of W^{183}.

Along these lines it would be interesting if an extensive coulomb excitation experiment were carried out on a sample of isotopically separated W^{183}. An electron spectrograph would then be needed to accurately measure the energies of the resulting conversion electrons. This experiment could prove conclusively whether or not the lowest state in Murray's level scheme[40] is the ground state of W^{183}.

3. Electric Dipole Transition Probabilities

Figures 8 and 9 show that E1 transition lifetimes calculated from Nilsson's wave functions[60] do give qualitative agreement with the experimental data. It is also noted that quantitative agreement cannot be claimed for specific nuclear transitions.

These calculations indicate that the lifetimes depend rather sensitively on the near cancellation of large terms in the matrix element. Thus, the rather erratic fluctuations in E1 transition rates from isotope to isotope are qualitatively understandable. Figures 8 and 9 illustrate this principal by showing how the calculated E1 transition lifetimes are affected by the two different assumed radial wave functions.

An interesting point to speculate on is the delayed nature of several of these transitions. Figure 7 shows that some of the E1 transitions are delayed by a factor of 10^5 from the simple Weisskopf estimate.[2, 3] It has already been mentioned that in the limit of small spheriodal deformation (this case corresponds to the spherical shell model) E1 transitions are hindered owing to a Δj forbiddenness.[72] It would be interesting to see if there are comparable selection rules acting to hinder E1 transitions in the limit of large prolate spheroidal deformations.

Nilsson[60] has indicated that in the limit of very large prolate deformation individual nucleonic states can be characterized by four quantum numbers. In Nilsson's notation these four quantum numbers are as follows:

N is the principal quantum number of the oscillator,

n_z is the quantum number of the oscillations along the nuclear symmetry axis,

Λ is the projection of the particle orbital angular momentum nuclear symmetry axis,

Σ is the projection of the intrinsic spin along the nuclear symmetry axis.

Note that the spin value of a particle state is given by

$$I_0 = \Omega = \Lambda + \Sigma. \tag{11}$$

Also the parity of the state is determined by whether N is odd or even. Hence

$$\pi = (-1)^N, \tag{12}$$

where $\pi = -1$ signifies an odd-parity state

and $\pi = +1$ signifies an even-parity state.

Nilsson[60] has given the method for obtaining these four quantum numbers for any particular state.

Alaga[86] has considered the role of these new quantum numbers in beta decay. A summary of Alaga's selection rules for allowed and first-forbidden beta transitions associated with these quantum numbers is given in Table III.

Alaga[86] has used these selection rules to classify many beta transitions in the region $150 < A < 190$. The comparison of experimental data with Alaga's theoretical classifications indicates that these beta selection rules are very useful for explaining certain features of beta-decay transition rates in the regions of strongly deformed nuclei.

Similarly, there are certain selection rules for E1 transitions. These selection rules are summarized in Table IV. K-selection rules have been discussed previously and are excluded from this discussion by the assumption that $K = \Omega$ for all cases considered.

Table III

Selection Rules for Allowed and First-Forbidden Beta Transitions ($K = \Omega$)

Beta Transition	Selection Rules	Parity Change
Allowed	$\Delta N = 0$, $\Delta n_z = 0$, $\Delta\Lambda = 0$, $\Delta\Omega = 0, \pm 1$	No
First Forbidden ($\Delta I = 0, \pm 1$)	$\Delta N = \pm 1$ $\Delta n_z = \pm 1$, $\Delta\Lambda = 0$, $\Delta n_z = 0$, $\Delta\Lambda = \pm 1$, $\Delta\Omega = 0, \pm 1$	Yes

Table IV

Selection Rules for Electric Dipole Transitions ($K = \Omega$)

Beta Transition	Selection Rules	Parity Change
$\Delta N = \pm 1$	$\Delta n_z = \pm 1$, $\Delta\Lambda = \Delta\Omega = 0$ $\Delta n_z = 0$, $\Delta\Lambda = \Delta\Omega = \pm 1$	Yes

In Table V we list the asymptotic quantum numbers (N, n_z, Λ, Ω) for some of Nilsson's orbitals.[60] Table VI summarizes the asymptotic quantum-number changes between states possibly involved in low-lying E1 transitions in the actinide region.

Thus, these E1 transitions are forbidden in the asymptotic limit because of the selection rules shown in Table IV. It can be shown that virtually all of the possible low-lying E1 transitions for odd-Z nuclei in the actinide region violate these selection rules. It has already been noted that, in the limit of small spheroidal deformation, the E1 transitions are forbidden because they violate Δj selection rules. Thus, it is only for the case of intermediate nuclear deformations that E1 transitions can occur, because in this instance the various quantum numbers are not "good" and mixing may occur in the nuclear states.

Figure 10 illustrates this situation pictorially. The ratio of the calculated reduced transition probability to the Weisskopf[2,3] single-particle estimate of the reduced transition probability is plotted on the ordinate axis and a function of the deformation parameter is plotted as the abscissa. At $\eta = 0$, the ratio is zero because of the Δj - forbiddenness, and at $\eta = \infty$, the ratio is again zero because of the asymptotic selection rules. At intermediate deformations the calculated reduced transition probability ratio has the values shown in Fig. 10.

Finally, it is interesting to note what states must be mixed to account for the existence of E1 transitions. Nilsson[60] has shown that in the limit of very strong deformations the spin-orbit term couples states that have the same N and Ω but differ by one unit in Λ and n_z. Likewise, the $\vec{\ell}^2$ term couples states that have the same N, Ω, and Λ but differ by two units in n_z.

Let us reconsider the E1 transition between states 55 and 44. Because of the spin-orbit term, Nilsson's state 36 may mix in with state 44.[60] From Tables IV and V we note that an E1 transition between states 55 and 36 is allowed. Likewise the $\vec{\ell}^2$ term will permit state 72 to mix with state 55. The E1 transition between states 72 and 44 is also an allowed transition by the asymptotic selection rules. Thus, we see how the delayed E1 transitions may

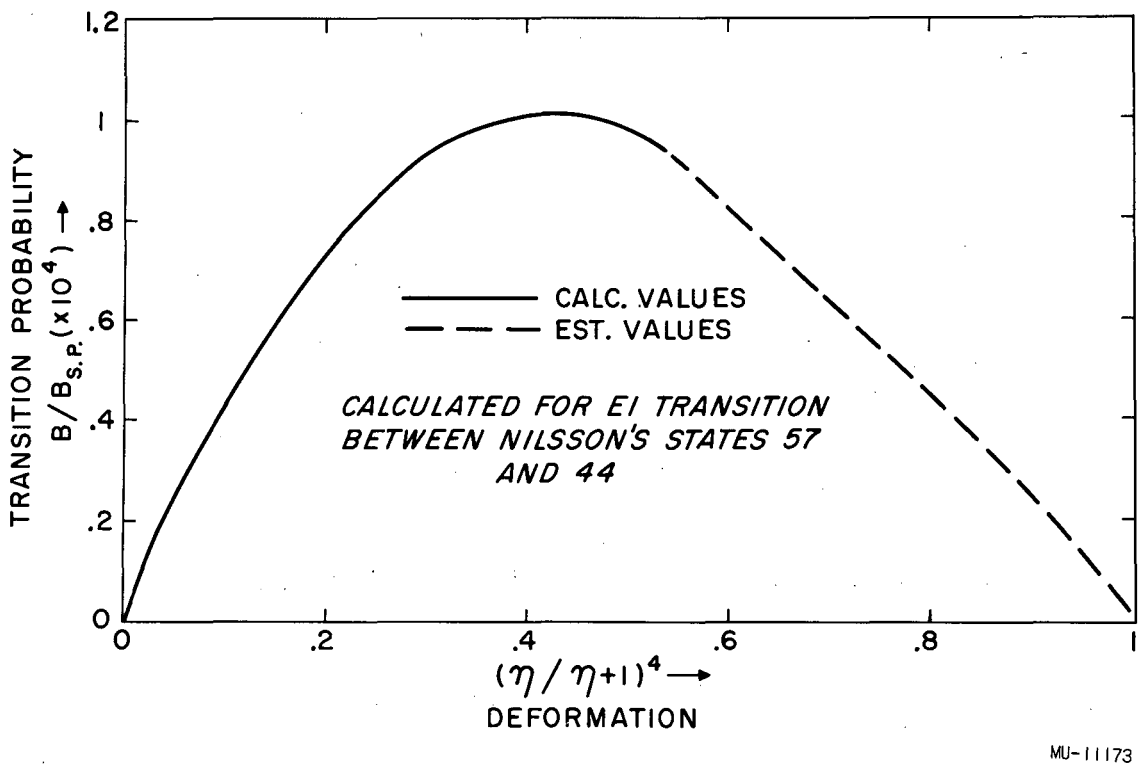

Fig. II-10 Pictorial Representation of an E1 Transition Probability as a Function of Deformation

Table V

Asymptotic Quantum Numbers for Nilsson's Orbits

Nilsson's Orbits	N	n_z	Λ	Ω
44	5	2	3	5/2
46	5	3	2	3/2
50	5	1	2	5/2
52	5	2	1	3/2
55	6	4	2	5/2
57	6	5	1	3/2
60	6	6	0	1/2
62	5	1	2	3/2
69	6	5	1	1/2
36	5	3	2	5/2
72	6	2	2	5/2

Table VI

Asymptotic Quantum Number Changes for Electric Dipole Transitions

Initial Orbit	Final Orbit	ΔN	Δn_z	$\Delta\Lambda$	$\Delta\Omega$
60	52	-1	-4	+1	+1
60	46	-1	-3	+2	+1
57	50	-1	-4	+1	+1
57	44	-1	-3	+2	+1
69	62	-1	-4	+1	+1
55	50	-1	-3	0	0
55	44	-1	-2	+1	0
55	52	-1	-2	-1	-1
55	46	-1	-1	0	-1

proceed through impurities in the nuclear states.

The amount of mixing in these states is expected to be very small, since states 44 and 36 and also states 55 and 72 are separated by a very large energy difference.

D. Acknowledgments

I wish to express my gratitude to Professor J. O. Rasmussen, whose continuous encouragement and guidance made this work possible.

I would like to thank Drs. M. I. Kalkstein, J. M. Hollander, F. Asaro, and F. S. Stephens for many helpful discussions.

The assistance of V. G. Ogren, W. Gantz, A. Larsh, and H. P. Robinson with the many electronics problems that have arisen is deeply appreciated.

I would like to express my appreciation to Professors G. T. Seaborg and I. Perlman for their helpful comments.

Drs. S. G. Thompson, B. G. Harvey, G. R. Choppin, A. Ghiorso, F. Asaro, F. S. Stephens, W. G. Smith, R. A. Glass, A. W. Stoner, A. R. Fritsch, J. P. Hummel, S. Thulin, Miss Virginia A. Schultz, Mr. C. J. Gallagher, Jr., and Mr. R. C. Pilger kindly supplied the activities used in these studies.

I would like to express my gratitude to Dr. F. K. McGowan of the Oak Ridge National Laboratory for helpful suggestions concerning the fast-coincidence circuiting and to C. W. Johnstone of the Los Alamos National Laboratory for supplying detailed photographs and information on construction of the single-channel pulse-height analyzer.

I am grateful to Dr. S. G. Nilsson, who made his wave functions available prior to publication.

Finally, the cooperation of the Health Chemistry Group, who made it possible to carry out this work with a minimum of radiation hazard, is gratefully acknowledged.

This work was performed under the auspices of the United States Atomic Energy Commission.

REFERENCES

1. Bay, Henri, and McLernon, Phys. Rev. 97, 561 (1955).
2. S. A. Moszkowski, Beta- and Gamma-Ray Spectroscopy, Interscience, New York, 1955, pp. 373-395.
3. J. M. Blatt and V. F. Weisskopf, Theoretical Nuclear Physics, Wiley, New York, 1952, p. 627.
4. M. Goldhaber and A. W. Sunyar, Beta- and Gamma-Ray Spectroscopy, Interscience, New York, 1955, pp. 453-467.
5. A. W. Sunyar, Phys. Rev. 98, 653 (1955).
6. A. Bohr and B. R. Mottelson, Kgl. Danske Videnskab. Selskab, Mat-fys. Medd. 27, No. 16 (1953); also Beta- and Gamma-Ray Spectroscopy, Interscience, New York, 1955, Chapter XVII, pp. 468-493.
7. P.H. Stelson and F. K. McGowan, Phys. Rev. 99, 112 (1955).
8. H.A. Bethe, Revs. Modern Phys. 9, 69 (1937), Sec. 88.
9. P. R. Bell, Beta- and Gamma-Ray Spectroscopy, Interscience New York, 1955, pp. 132-164.
10. M. I. Kalkstein and J. M. Hollander, "A Survey of Counting Efficiencies for a 1.5-Inch Diameter by 1-Inch High Sodium Iodide (Thallium Activated) Crystal," University of California Radiation Laboratory Unclassified Report UCRL-2764, Oct. 1954.
11. C. W. Johnstone, Nucleonics 11, 36 (1953).
12. A. Ghiorso and A. E. Larsh, in Chemistry Division Quarterly Report, UCRL-2647, July 1954.
13. Bell, Graham, and Petch, Can. J. Phys. 30, 35 (1952).
14. Z. Bay, Phys. Rev. 77, 418 (1950).
15. T. D. Newton, Phys. Rev. 78, 490 (1950).
16. Bay, Henri, and Kanner, Phys. Rev. 100, 1197 (1955).
17. Beling, Newton, and Rose, Phys. Rev. 87, 670 (1952).
18. F. S. Stephens, "Decay Schemes and Nuclear Spectroscopic States in the Heavy-Element Region" (Thesis), University of California Radiation Laboratory Unclassified Report UCRL-2970, June 1955.
19. D. Engelkemeir and L. B. Magnusson, Phys. Rev. 94, 1395 (1954).
20. Teillac, Rious, and Desneiges, Compt. rend. 237, 41 (1953).
21. D. Engelkemeir and L. B. Magnusson, Phys. Rev. 99, 135 (1955).
22. cf. Table of Isotopes, Hollander, Perlman, and Seaborg, Revs. Modern Phys. 25, 469 (1953).

23. Street, Ghiorso, and Seaborg, Phys. Rev. 79, 530 (1950).
24. F. Asaro and I. Perlman, Phys. Rev. 93, 1423 (1954).
25. M. I. Kalkstein and J. O. Rasmussen, unpublished results, 1953.
26. D. Engelkemeir, private communication, 1955.
27. J. O. Rasmussen and F. S. Stephens, unpublished data, 1953.
28. Freedman, Jaffey, Wagner, and May, Phys. Rev. 89, 302 (1952).
29. Hoff, Olsen, and Mann, "Electron Capture and Alpha Decay of Np^{235}," University of California Radiation Laboratory Un-Classified Report UCRL-4517, Jan. 1956.
30. Diamond, Magnusson, Mech, Stevens, Friedman, Studier, Fields, and Huizenga, Phys. Rev. 94, 1083 (1954).
31. F. Asaro, private communication, (1956).
32. E. K. Hyde, Phys. Rev. 94, 1221 (1954).
33. R. C. Pilger, private communication, (1956).
34. J. O. Rasmussen and E. K. Hyde, unpublished results, (1953).
35. Magnusson, Wagner, Engelkemeir, and Freedman, "Radiations of Tl^{209}, Pb^{209}, Bi^{213}, and Ra^{225}," Argonne National Laboratory Unclassified Report ANL-5386, Jan. 1955.
36. Perlman, Stephens, and Asaro, Phys. Rev. 98, 262A (1955).
37. R. L. Graham and R. E. Bell, Phys. Rev. 83, 222 (1951).
38. Hollander, Smith, and Mihelich, Phys. Rev. 100, 1238A (1955); also Phys. Rev., in press(1956).
39. Thulin, Rasmussen, Gallagher, Smith, and Hollander, Phys. Rev., to be published, (1956).
40. Murray, Boehm, Marmier, and DuMond, Phys. Rev. 97, 1007 (1955).
41. J. P. Hummel, unpublished data, (1956).
42. D. Wilkinson and H. G. Hicks, Phys. Rev. 77, 314 (1950).
43. McClelland, Mark, and Goodman, Phys. Rev. 93, 904 (1954).
44. T. Huus and J. H. Bjerregaard, Phys. Rev. 92, 1579 (1953).
45. W. G. Smith and J. M. Hollander, Phys. Rev. 101, 746 (1956).
46. F. D. S. Butement and A. J. Poë, Phil. Mag. 46, 482 (1955).
47. M. E. Rose, Beta- and Gamma-Ray Spectroscopy, Interscience, New York, 1955, Appendix IV; and privately circulated tables.

48. A. M. Lane and D. H. Wilkinson, Phys. Rev. 97, 1199 (1955).
49. J. A. Harvey, Can. J. Phys. 31, 278 (1953).
50. Sunyar, Mihelich, Scharff-Goldhaber, Goldhaber, Wall, and Deutsch, Phys. Rev. 86, 1023 (1952).
51. A. de Shalit and M. Goldhaber, Phys. Rev. 92, 1211 (1953).
52. R. W. King and D. C. Peaslee, Phys. Rev. 94, 1284 (1954).
53. Alaga, Alder, Bohr, and Mottelson, Kgl. Danske Videnskab. Selskab Mat-fys. Medd. 29, No. 9 (1955).
54. E. U. Condon and G. H. Shortley, The Theory of Atomic Spectra, University Press, Cambridge, 1935.
55. A. Simon, "Numerical Table of the Clebsch-Gordan Coefficients," Oak Ridge National Laboratory Unclassified Report ORNL-1718, June 1954.
56. Divatia, Davis, Moffat, and Lind, Phys. Rev. 100, 1266A (1955); also verbal report.
57. Novey, Freedman, Porter, and Wagner, "Beta Gamma Directional Correlation in Re^{186}," Argonne National Laboratory Unclassified Report ANL-5523, Feb. 1956.
58. J. P. Hurley and P. S. Jastram, Phys. Rev. 95, 627A (1954).
59. M. G. Mayer and J. H. D. Jensen, Elementary Theory of Nuclear Shell Structure, Wiley, New York and London, 1955.
60. S. G. Nilsson, Kgl. Danske Videnskab. Selskab, Mat-fys. Medd. 29, No. 16 (1955).
61. B. R. Mottelson and S. G. Nilsson, Phys. Rev. 99, 1615 (1955).
62. Manning, Fred, and Tomkins, Abstracts of Spectroscopy Symposium at Argonne National Laboratory, (Feb. 1956).
63. B. R. Mottelson and S. G. Nilsson, Z. Physik 141, 217 (1955).
64. Bleaney, Llewellyn, Pryce, and Hall, Phil. Mag. 45, 773 (1954).
65. J. E. Mack, Revs. Modern Phys. 22, 64 (1950).
66. F. Asaro and I. Perlman, Phys. Rev. 88, 828 (1952).
67. Freedman, Wagner, and Engelkemeir, Phys. Rev. 88, 1155 (1952).
68. Bleaney, Llewellyn, Pryce, and Hall, Phil. Mag. 45, 991 (1954).
69. P. B. Sogo and C. D. Jeffries, Phys. Rev. 98, 1316 (1955).
70. Bleaney, Llewellyn, Pryce, and Hall, Phil. Mag. 45, 992 (1954).
71. F. S. Tomkins, Phys. Rev. 73, 1214 (1948).

72. J. O. Rasmussen, Arkiv Fysik 7, 185 (1953).
73. J. S. Fraser and J. C. D. Milton, Phys. Rev. 94, 795A (1954).
74. Krohn, Novey, and Raboy, Phys. Rev. 98, 1187A (1955).
75. J. O. Rasmussen, unpublished calculations, 1955.
76. J. G. Conway and R. D. McLaughlin, unpublished data, 1954.
77. M. Fred and F. S. Tomkins, Phys. Rev. 89, 318 (1953).
78. J. G. Conway and R. D. McLaughlin, Phys. Rev. 94, 498 (1954).
79. Asaro, Reynolds, and Perlman, Phys. Rev. 87, 277 (1952).
80. Hollander, Smith, and Rasmussen, Phys. Rev., in press, (1956).
81. Engelkemeir, Fields, and Huizenga, Phys. Rev. 90, 6 (1953).
82. R. W. Hoff and L. Mann, unpublished data, 1955.
83. D. M. Chase and L. Wilets, Phys. Rev. 101, 1038 (1956).
84. H. de Waard, Phil. Mag. 46, 445 (1955).
85. J. G. Conway and R. D. McLaughlin, Phys. Rev. 96, 541 (1954).
86. G. Alaga, Phys. Rev. 100, 432 (1955).